Synergistic Regulation of Notch Signaling by Different O-Glycans Promotes Hematopoiesis

Ankit Tanwar,[1] Pamela Stanley[1]*

[1]Dept. Cell Biology, Albert Einstein College of Medicine, New York, NY, USA

*Corresponding author. Email: pamela.stanley@einsteinmed.edu

Abstract: Glycosylation of Notch receptors by O-fucose glycans regulates Notch ligand binding and Notch signaling during hematopoiesis. However, roles in hematopoiesis for other O-glycans that modify Notch receptors have not been determined. Here we show that the EGF domain specific GlcNAc transferase EOGT is required in mice for the optimal production of lymphoid and myeloid cells. The phenotype of *Eogt* null mice was largely cell-autonomous, and Notch target gene expression was reduced in T cell progenitors. Moreover, EOGT supported residual Notch signaling following conditional deletion of *Pofut1* in hematopoietic stem cells (HSC). *Eogt:Pofut1* double mutant HSC had more severe defects in bone marrow, and in T and B cell development in thymus and spleen, compared to deletion of *Pofut1* alone. The combined results show that EOGT and O-GlcNAc glycans are required for optimal hematopoiesis and T and B cell development, and that they act synergistically with POFUT1 and O-fucose glycans to promote Notch signaling in lymphoid and myeloid differentiation.

One Sentence Summary: O-GlcNAc glycans and EOGT promote lymphopoiesis and myelopoiesis and support Notch signaling in the absence of POFUT1 and O-fucose glycans.

INTRODUCTION

Notch signaling is highly conserved and plays crucial roles in cell fate determination and tissue development (*1, 2*). There are four Notch receptors (NOTCH1 to NOTCH4) that can be activated by five canonical Notch ligands (DLL1, DLL3, DLL4, JAG1 and JAG2) to induce Notch signaling in mammals. Notch ligand binding and Notch signaling are regulated by glycosylation of the extracellular domain (ECD) of Notch receptors (*3, 4*). Structural studies of a NOTCH1 ECD ligand-binding fragment co-crystallized with an N-terminal fragment of DLL4 or JAG1 reveal direct interactions between Notch ligands and O-fucose in specific epidermal growth factor-like (EGF) repeats of NOTCH1 (*5, 6*). Following Notch ligand engagement with Notch receptor, an ADAM metalloprotease cleaves NECD, followed by a second cleavage within the membrane by the γ-secretase complex. Notch intracellular domain (NICD) travels to the nucleus where, in complex with the transcriptional repressor Rbp-Jk, the co-activator Mastermind-like-1 (MAML1), and other co-activators, the complex induces expression of Notch target genes, including Hairy enhancer-of-split (*Hes*) and Hairy-related (*Hey* or *Hrt*) gene families, which regulate the expression of many other genes (*2, 7*).

Within the hematopoietic system, Notch signaling plays important roles in regulating different stages of lymphoid and myeloid development (*8, 9*). It is now clear that DLL4-induced NOTCH1 signaling is indispensable for T cell development in the thymus. Thus, conditional inactivation of *Notch1* or *Dll4* using *Mx1-Cre* is sufficient to block T cell development (*10, 11*). However, *Notch2* is also required for optimal development of early T cell progenitors (*12*). DLL1-induced NOTCH2 signaling is essential for the generation of marginal zone B cells (MZ-B) in the spleen (*13, 14*). O-fucose glycans extended by (*15*)LFNG and MFNG together promote the formation of MZ-B cells (*16*).

Consensus sites within EGF repeats in the NECD of Notch receptors are decorated with O-fucose, O-glucose and O-GlcNAc glycans (*17*) (Fig. 1). EGF repeats with appropriate consensus sites occur in ~100 proteins of the proteome, including the four Notch receptors and five Notch ligands (*18, 19*). O-fucose is transferred by protein O-fucosyltransferase 1 (POFUT1), which is further extended by the *Fringe* family of glycosyltransferases (LFNG, MFNG and RFNG). Misexpression of *Lfng* in thymus disrupts T cell development (*20-22*). Conditional deletion of *Pofut1* in the bone marrow via *Mx1-Cre* or *Vav1-iCre* leads to the disruption of hematopoiesis with an increase in granulocyte-monocyte progenitors (GMP), and a reduction in common myeloid progenitors (CMP) (*23*). This results in a block in T cell production in thymus, and a block in MZ-B cell production in spleen, accompanied by reduced T cells and an increase in granulocytes. Notch ligand binding and Notch signaling in hematopoietic stem cells (HSC) are markedly reduced following conditional deletion of *Pofut1*. Embryonic lethality follows global deletion of *Pofut1* (*24, 25*), or *Notch1* (*26, 27*), or the downstream effector of Notch signaling RBP-Jk (*28*). Thus, it is surprising that conditional deletion of *Pofut1* in HSC gives a milder reduction in thymic T cells than deletion of RBP-Jk by *Mx1-Cre* (*29*). This result indicates that loss of O-fucose glycans from NOTCH1 in HSC does not fully abrogate NOTCH1 signaling, and suggests that other O-glycans on NOTCH1 may support Notch signaling in the absence of POFUT1. Synergism between O-fucose and O-glucose glycans on Notch has been observed in *Drosophila* (*30*), and in mammalian cells (*31*). However, in both cases, the effects on Notch signaling appear to be due to reduced expression of Notch receptors lacking O-fucose and O-glucose glycans at the cell surface. By contrast, the absence of O-fucose glycans from Notch receptors in CHO cells only slightly reduces NOTCH1 cell surface levels (*32*).

The addition of O-GlcNAc to EGF repeats was first identified in *Drosophila* (*33*), and an EGF domain specific O-GlcNAc transferase (EOGT) was subsequently identified (*34, 35*). Genetic interactions between *Drosophila eogt* and Notch pathway members were reported (*35*). *Eogt* null mice are viable and fertile, but exhibit defective postnatal retinal angiogenesis, similar to that observed in mice with disrupted DLL4-NOTCH1 signaling (*36*). Cell-based experiments showed that EOGT promotes the binding of DLL Notch ligands and Notch signaling (*36*). RNA-seq data show that *Eogt* is expressed with *Pofut1* in many cells of the immune system (Fig. 1). However, their expression levels vary inversely in some cell types, indicating potentially different functional roles (Fig. 1). In this paper, we identify roles for EOGT and O-GlcNAc glycans in the regulation of Notch signaling during hematopoiesis, lymphopoiesis and

myelopoiesis. In addition, we show that O-GlcNAc glycans initiated by EOGT support Notch signaling in the absence of POFUT1 and O-fucose glycans.

RESULTS

Loss of *Eogt* affects myelopoiesis and lymphopoiesis

To investigate roles for EOGT and O-GlcNAc glycans in the differentiation of HSC, the frequency of different lymphoid and myeloid subsets in bone marrow, thymus and spleen cells, as well as absolute cell number differences, were determined. Gating strategies for bone marrow, thymus and spleen cell populations are shown in figs. S1, S2 and S3, respectively. Initial comparisons of *Eogt*[+/+] and *Eogt*[+/-] heterozygotes revealed no significant differences in the absolute number of bone marrow cells, or the ratio of thymus:body or spleen:body weight, respectively (fig. S4A). T, B and myeloid cell subsets from bone marrow (fig. S4B), thymus (fig. S4C) and spleen (fig. S4D) from *Eogt*[+/+] and *Eogt*[+/-] mice showed no significant differences in absolute cell numbers, or the proportions of lymphoid and myeloid cell subsets (fig. S4B-D and not shown). Therefore, *Eogt*[+/+] and *Eogt*[+/-] were combined as Control and compared to *Eogt* null mice. Thymus and spleen weights as well as bone marrow (BM) cellularity were similar in *Eogt* null and Control mice (fig. S5A).

In bone marrow, the number of immature B cells (CD19+), more mature CD19/B220+ and B220+ B cells, and granulocytes (Gr-1+) were all significantly increased in the *Eogt*[-/-] population, whereas the number of myeloid cells (CD11b+) was markedly decreased (Fig. 2A). In thymus, the proportion of CD4/CD8 double negative (DN) DN1, and the absolute cell number of DN2 T cell progenitors, were strikingly reduced in *Eogt* null cells, while the proportion of DN4 T cells was significantly increased (Fig. 2B). By contrast, the numbers of early T cell progenitors (ETP) and DN3 T cells were unchanged (fig. S5B). The proportion of double positive (DP) T cells was slightly decreased, while CD4+ and CD8+ single positive (SP) T cells were increased in *Eogt*[-/-] thymocytes (Fig. 2B). These effects were very similar to the T cell phenotype observed in mice lacking the three Fringe genes (*Fng* tKO) (*37, 38*). Consistent with inhibition of Notch signaling in the *Eogt* null thymus, there was a significant increase in the absolute numbers of thymic B cells (CD19/B220+) and myeloid cells (CD11b+) (Fig. 2B). However, the natural killer (NK) T cell population (NK1.1+) did not change compared to Control (fig. S5B). In spleen, no histopathological changes were observed Control versus *Eogt*[-/-] mice, the absolute number of CD4+ and CD8+ T cells, B cells (CD19/B220+), marginal zone progenitors (MZ-P) and myeloid cell subsets were similar in Control versus *Eogt*[-/-] mice (fig. S5C). However, significant increases were observed in the number of follicular B (Fo-B), MZ-B, CD19+ and B220+ B cells in splenocytes of *Eogt*[-/-] mice (Fig. 2C). By contrast, a decrease in the proportion of natural killer T cells (NK1.1+) and of dendritic cells (CD11b/c+) was observed (Fig. 2C). Thus, EOGT and O-GlcNAc glycans are required for the optimal generation of lymphoid and myeloid cells from HSC.

The *Eogt* null phenotype is largely cell autonomous

To determine whether changes in *Eogt* null T, B and myeloid cell subsets were cell intrinsic, bone marrow (BM) transplantation was performed from CD45.2+ *Eogt*[+/-] and *Eogt*[-/-] donor mice into CD45.1+ male hosts. *Eogt*[-/-] CD45.2+ donor BM cells reconstituted CD45.1+ hosts to a level of ~59% in bone marrow (Fig. 3A), ~80% in thymus and ~64% in spleen (not shown). Thus, host-derived *Eogt*[+/+] cells contributed to each of these cell populations. In recipient bone marrow, myeloid cells (CD11b+) arising from *Eogt*[-/-] donor BM were reduced compared to CD11b+ cells from *Eogt*[+/-] BM (Fig. 3B); in recipient thymus, *Eogt*[-/-] donor BM generated significantly fewer DN2 and DN3 T cell progenitors compared to *Eogt*[+/-] donor BM (Fig. 3C); and in spleen, *Eogt*[-/-] donor BM generated CD19+ cells and Gr-1+ granulocytes in significantly increased numbers compared to *Eogt*[+/-] donor BM (Fig. 3D). Thus, while the altered phenotype of *Eogt*[-/-] immune cell subsets was largely transferred, the phenotype of *Eogt*[-/-] BM recipients was somewhat milder, and did not exhibit all aspects of the *Eogt* null phenotype (Fig. 3B). This could reflect the fact that *Eogt*[+/+] host cells contributed to the bone marrow in CD45.1 hosts, and/or that the wild type stroma of CD45.1 hosts rescued some of the deficiencies of *Eogt*[-/-] cells. Nevertheless, key aspects of the *Eogt* null phenotype were transferred by *Eogt*[-/-] BM.

Notch signaling is reduced in *Eogt*[-/-] DN T cell progenitors

Notch ligand binding was examined using thymic DN T cell progenitors from 7-8 week old *Eogt*[+/-] and *Eogt*[-/-] mice. No significant changes were observed in either NOTCH1 cell surface expression, or the binding of soluble ligands DLL1, DLL4, JAG1 or JAG2 between Eogt[+/-] and *Eogt*[-/-] DN T cell progenitors (Fig. 4A). However, there were significant reductions in the expression of two Notch target genes, *Hes1* and *Il2ra,* consistent with reduced Notch signaling (Fig. 4B). The expression of *Il2ra* was also reduced in DN T cell progenitors from mice lacking the three Fringe genes, along with *Dtx1,* although not *Hes1* (*37*). The reduction in Notch signaling target gene expression in *Eogt* null T cell progenitors, the changes in T cell subset numbers and frequencies, and the increased numbers of B and myeloid cells observed in *Eogt*[-/-] thymus, indicate that EOGT and O-GlcNAc glycans are necessary for optimal Notch signaling and T cell development. The altered B cell and myeloid subsets in spleen of *Eogt*[-/-] mice are also consistent with reduced Notch signaling. Finally, the B cell and myeloid hyperplasia in *Eogt*[-/-] BM indicate that Notch signaling is required for regulating the differentiation of certain progenitors during hematopoiesis.

Eogt* supports lymphoid and myeloid development in HSC lacking *Pofut1

Previous work showed that inactivation of *Pofut1* using *Mx1-Cre* causes a reduction in T lymphopoiesis in thymus and myeloid hyperplasia in bone marrow (*23*). In another study, deletion of *Pofut1* was shown to cause a milder hematopoietic phenotype than deletion of RBP-Jk (*29*). To determine whether *Eogt* and O-GlcNAc glycans support Notch signaling and hematopoiesis in the absence of *Pofut1*, we used *Vav1-iCre* transgenic mice to generate conditional deletion (cKO) of *Pofut1* (henceforth referred to as Pof cKO), and deletion of both *Eogt* and *Pofut1* (henceforth referred to as EPof dKO), in hematopoietic stem cells. The absolute

number of BM cells was significantly increased in both Pof cKO and EPof dKO mice (Fig. 5). Gating strategies used to define HSC, HSPC, myeloid and lymphoid cell subsets in BM are shown in fig. S6. Short-term (ST)-HSC, LSK (Lineage-Sca1+cKit+) and Lin-Sca1+ populations were increased in both Pof cKO and EPof dKO mutants, but HSPCs were increased only in EPof dKO BM (Fig. 5). By contrast, MPP subsets were reduced except for a small increase in MPP3 cells in EPof dKO BM (Fig. 5). Lymphoid primed multipotent progenitor cell (MPP4/LMPP) and common myeloid precursors (CMP) were reduced in Pof cKO and further reduced in EPof dKO BM, and megakaryocytes erythrocytes progenitors (MEP) were decreased in both single and double mutants (Fig. 5). By contrast, granulocyte-monocyte progenitors (GMP) were increased in Pof cKO (as observed previously (*23*)), and further increased in EPof dKO BM (Fig. 5 and fig. S7). CD11b+ myeloid cells and CD11b+/Gr-1+ myeloid-derived suppressor cells (MDSC) were increased, but common lymphoid progenitors (CLP) were reduced in EPof dKO BM (Fig. 5). B cells in BM (CD19+, B220+ and CD19/B220+) were also decreased in EPof dKO mice (Fig. 5). NOTCH1 was expressed at the surface of Lin-Sca1+ cells which were increased in frequency in Pof cKO and EPof dKO BM (fig. S8). Binding of DLL1 and DLL4 Notch ligands was low and similar in control and mutant Sca1+ cells (fig. S8).

Highly disrupted development of T cells in EPof dKO thymus

Deletion of *Pofut1* in HSC via *Vav1-iCre* led to a marked decrease in thymus weight and a similar reduction was observed in EPof dKO thymus (Fig. 6A). The reduced size was accompanied by a dramatic change in T cell maturation (Fig. 6B). Early thymic progenitors (ETP) were greatly decreased, and each DN T cell progenitor population (DN1 to DN4) was reduced in absolute cell number in Pof cKO, and even further reduced in EPof dKO thymocytes (Fig. 6C and fig. S8). Interestingly, however, the proportion of DN4 T cells in both single and double mutant thymocytes was increased relative to control (fig. S9), as observed in thymus lacking all Fringe activities (*37*). The DN thymic population, which includes few if any DN T cell progenitors and all non-T cell populations, was greatly increased in Pof cKO and EPof dKO. This reflected loss of Notch signaling leading to the generation of B cells, myeloid and NK cell subsets (Fig. 6D and fig. S9). The fact that effects were more severe in EPof dKO than Pof cKO thymus, however, indicates that the loss of Notch signaling was greater in EPof dKO thymus.

Defective B, T and myeloid cell development in EPof dKO spleen

Both Pof cKO and EPof dKO mice had an enlarged spleen (Fig. 7A). Absolute numbers of splenocytes and spleen weight were increased in Pof cKO, and more increased in EPof dKO mice (Fig. 7B). Histological analysis revealed extramedullary hematopoiesis in both Pof cKO and EPof dKO spleen, with larger areas of extramedullary hematopoiesis observed in EPof dKO spleen (Fig. 7A).

The proportion of CD4+ T and CD8+ T cells were significantly reduced in Pof cKO, and further reduced in EPof dKO spleen (Fig. 7C and fig. S10). While CD19+ and B220+ B cells were increased in both Pof cKO and EPof dKO spleen, the CD19+/B220+ B cell population was reduced (Fig. 7D). The frequency of Fo-B and and the number of MZ-B cells were reduced (Fig.

7D and fig. S10). While the absolute number of MZ-P cells did not change in the mutants, the relative frequency of MZ-P precursors increased in EPof dKO spleen (Fig. 7 and fig. S10). Myeloid cell subsets such as dendritic cells (CD11b/c+) and Gr-1+ granulocytes were increased in a greater proportion in EPof dKO compared to Pof cKO spleen. However, natural killer T (NK1.1) cell were decreased in frequency in both Pof cKO and EPof dKO spleen (Fig. 7D and fig. S10).

DISCUSSION

Defining specific roles for the glycans that regulate Notch signaling in lymphoid and myeloid development facilitates our understanding of cell fate decisions controlled by Notch signaling, and potential consequences for people with congenital diseases that perturb Notch signaling. Several congenital diseases inhibit the synthesis or extension of O-glycans that regulate Notch signaling and may induce immune cell defects. Mutations in *EOGT* cause Adams Oliver syndrome or EOGT-CDG (*15*) and autosomal dominant mutations in *POFUT1* cause Dowling Degos Disease 2 (DDD2) or POFUT1-CDG (*39*). Here we show that the generation of certain lymphoid and myeloid subsets in bone marrow, thymus and spleen were perturbed in mice lacking *Eogt*. In the bone marrow, loss of EOGT caused increased numbers of immature B cells and Gr-1+ myeloid cells, but a reduction in CD11b+ myeloid cells. In thymus, the phenotype of *Eogt* null mice was similar, but not identical to, mice which lack all three Fringe genes (*Fng* tKO) (*37*). Early T cell progenitors DN1 and DN2 were reduced in frequency, whereas DN4 T cell progenitors were increased, DP T cells were slightly reduced, and CD4+ and CD8+ SP T cells were increased. Inhibition of Notch signaling in thymus is well known to lead to the generation of B cells and myeloid cells in place of T cells (*9, 11, 40, 41*). *Eogt* null thymus contained significantly increased numbers of B cells and granulocytes, and an increased frequency of myeloid cells. In spleen, *Eogt* null splenocytes exhibited increased numbers of several B cell subsets, although no effects on CD4+ or CD8+ T cell numbers. This indicates that T cells that left the *Eogt* null thymus were not compromised, unlike in *Fng* tKO mice which had a reduced frequency of T cells in spleen (*37*). Deletion of RBP-Jk by *Vav1-iCre* results in an increased frequency of CD19+ B cells (*42*), also observed in *Eogt* null spleen. *Eogt* null mice showed increased absolute numbers of CD19+ B-cells, increased Fo-B cells, and a decrease in natural killer T-cells (NK1.1+) and dendritic cells (CD11b/c+) in the spleen. The overall *Eogt* null phenotype was largely cell autonomous following bone marrow transplantation. In addition, expression of Notch target genes *Hes1* and *Il2ra* was reduced, similar to *Fng* tKO DN T cell progenitors that had reduced *Il2ra* and *Dtx1* expression (*37*). The combined data provide strong evidence that EOGT and O-GlcNAc glycans are required for optimal Notch signaling in the development of lymphoid and myeloid cells from HSC(*43*).

Further evidence that EOGT and O-GlcNAc glycans support Notch signaling in lymphoid and myeloid development was obtained in compound mutant mice lacking *Eogt* and conditionally lacking *Pofut1* in HSC. We observed significant differences between Pof cKO and EPof dKO

lymphoid and myeloid populations in BM, thymus and spleen (Figs. 5-7). We conclude that the loss of *Eogt* and O-GlcNAc glycans in Pof cKO HSC exacerbated the deficits in T, B and myeloid differentiation evident in Pof cKO mice. This result, and our findings that *Eogt* is required for optimal Notch signaling and the differentiation of HSC, provide an explanation for the observation that *Pofut1*:*Mx1-Cre* T cell deficiencies were not as severe as those obtained in *RBP-Jk:Mx1-Cre* thymus (*29*). In the absence of POFUT1 and O-fucose glycans, the O-GlcNAc glycans transferred by EOGT to Notch receptors can support a low but significant level of Notch signaling. Thus, the O-fucose and O-GlcNAc glycans on Notch act synergistically to provide optimal Notch signaling in lymphopoiesis and myelopoiesis.

The conclusions obtained from these experiments are necessarily limited by the difficulty of demonstrating structural changes in the O-glycans on Notch receptors predicted to change in the absence of relevant glycosyltransferase(s). In addition, further investigations of roles for O-glycans in the regulation of T and B cell development should determine the effects of conditional deletion of *Eogt* in HSC to define the contribution, if any, of *Eogt* null stroma to the *Eogt* null phenotpye. It would also be important to determine Notch ligand binding and Notch target gene expression in cells from different HSPC lineages in Pof cKO and EPof dKO mice. Single cell RNA-seq of different mutant HSC and HSPCs would greatly expand our understanding of the pathways affected by altered Notch signaling due to loss of regulation by O-glycans in HSC. Roles in hematopoiesis for the O-glucose glycans on Notch receptors are also unknown. Finally, it would be important to investigate roles for the O-glycans on Notch ligands by deleting *Pofut1*, *Eogt* and related glycosyltransferase genes in stromal cells.

MATERIALS AND METHODS

Study Design

This study was designed to determine if EOGT and O-GlcNAc glycans are required for Notch signaling and its roles in the development of lymphoid and myeloid cells. First, we aimed to characterize immune cell subsets and Notch signaling in a global *Eogt* knockout mouse and to determine if any defects were cell autonomous by bone marrow transplantation. Second, we determined if HSC in mice with a conditional deletion of *Pofut1* and O-fucose glycans were supported by the presence of EOGT and O-GlcNAc glycans. Numbers of mice in each experiment were generally ≥6 per group and are shown as symbols in figures. Experimenters were not blinded to mouse experimental groups.

Mice

Mice with an inactivating mutation in the *Eogt* gene were previously described (*36*). *Pofut1*[F/F] mice were also previously described (*24*). Transgenic mice expressing *Vav1-iCre* (B6.Cg-*Commd10*$^{Tg(Vav1\text{-}icre)A2Kio}$/J Strain) were a kind gift from the Britta Will and Paul Frenette labs at the Albert Einstein College of Medicine, NY, USA. Compound mutant mice Pof cKO and EPof dKO with and without *Vav1-iCre* were generated by intercrossing. C57Bl/6J male congenic mice

expressing CD45.1 (*B6.SJL-Ptprc^a Pepc^b*/BoyJ *#002014*) were obtained from the Jackson Laboratory (Bar Harbor). Genotyping was performed by PCR of genomic DNA using primers that distinguish wild-type and mutant alleles (table S1). Mice were housed in a barrier facility, allowed to eat and drink ad libitum, and used in experiments at 7–8 weeks of age. All experiments were performed with permission from the Albert Einstein Institutional Animal Care and Use Committee under approved protocol numbers 20170709 and 00001311. Euthanized mice were weighed, and isolated thymus and spleen were also weighed before making single-cell suspensions.

Antibodies

Table S2 has the full description and commercial source of each antibody used in this work.

Flow cytometry

Single-cell suspensions from bone marrow were prepared by crushing both femurs, tibias, fibulae, patullae using a mortar and pestle and rinsing in 20 ml cold FACS binding buffer (FBB) with a glass pipette. FBB comprised Hank's balanced salt solution (HBSS) with glucose (Corning), 1 mM $CaCl_2$, 2% bovine serum albumin (BSA, fraction V, Sigma) and 0.05% sodium azide, pH 7.2–7.4. Bones were washed by extensive pipetting. The BM cell suspension in 20 ml cold FBB was passaged through a 70-µm strainer. Thymus or spleen were placed on a 70 µm strainer in 1 ml FBB, and homogenized with the head of the plunger of a 3-ml syringe. After passage through the 70-µm strainer, thymocytes were washed in 10 ml cold FBB twice, resuspended in 5 ml FBB, and counted in a Coulter counter (Beckman). Bone marrow and splenocytes were centrifuged and incubated in 1 ml RBC lysis buffer (eBiosciences) for 3-5 min before adding 10 ml cold FBB. After centrifugation and resuspension in 5 ml cold FBB, single cell suspensions were counted in a Coulter counter. Cells were centrifuged at 4ºC, resuspended in 2 ml cold PBS with 1 mM $CaCl_2$ and 1 mM $MgCl_2$, pH 7.2, centrifuged and resuspended in 100 µl Zombie NIR dye for live/dead assessment, according to the manufacturer's protocol (Zombie NIR Fixable Viability Kit, BioLegend). After 30 min incubation at 4ºC in the dark, 2 ml cold FBB was added. Cells were centrifuged at 4ºC and the cell pellet was resuspended in 4% paraformaldehyde (PFA) (Emsdiasum) in PBS pH 7.2, incubated 15 min at 4ºC in the dark. Cells were then centrifuged and washed twice with 2 ml cold FBB. Cells were resuspended at 10^6 cells/ml in FBB and stored at 4ºC for up to 3 months. For analysis by flow cytometry, ~$1x10^6$ cells were washed with 1 ml FBB, resuspended in 90 µl FBB containing 1 µl Fc block (rat-anti-mouse CD16/CD32), and incubated for 15 min on ice. Ab diluted in FBB (10 µl) was added and the reaction mix was incubated for 30 min at 4°C. Cells were washed twice in 1 ml FBB and resuspend in ~500 µl FBB. For all samples, immunofluorescence was analyzed using a Cytek™ Aurora flow cytometer and data FCS files were analyzed using FlowJo software (Tree Star). Gating strategies are explained in figs. S1, S2, S3 and S6 and are based on previously published gating methods (*37, 44, 45*).

Bone marrow transplantation

Cell suspensions were made from bone marrow by crushing the femurs, tibias, fibulae, patullae using a mortar and pestle of 7–8 week *Eogt*[+/-] and *Eogt*[-/-] male mice and rinsed with 20 ml cold HBSS, centrifuged and resuspended in RBC lysis buffer. After 3-5 min on ice, 10 ml HBSS was added, and the cells were washed three times in HBSS and counted in a Coulter counter (Beckman). Approximately 3 x10^6 cells from each mouse were resuspended in 50 µl HBSS (Gibco) and injected using 28-gauge insulin needle via the retro-orbital plexus into CD45.1+ C57BL/6 lethally irradiated recipients. A split dose of γ-Irradiation at 550 rad per recipient mouse was given twice, with a 16 h interval. After 7 weeks, recipient male mice were euthanized, bone marrow, thymus, and spleen were weighed, and single-cell suspensions were analyzed for lymphoid and myeloid cell subsets by flow cytometry after gating on donor-derived cells that were positive for staining with anti-CD45.2-Pacific Blue.

Isolation of CD4/CD8 DN T cells

Fresh thymocytes were resuspended in isolation buffer (PBS CMF, pH 7.2-7.4, containing 0.1% BSA, 2 mM EDTA and 1mg/ml glucose) on ice. For CD4+/CD8+ T cell depletion, ~3-5x10^7 thymocytes were incubated with 20 µg anti-CD4 (rat IgG2b clone GK1.5, BioXCell) and 37.5 µg anti-CD8a (rat IgG2a clone 53-6.72; BioXCell) in 5 ml isolation buffer for 20 min at 4°C with tilted rotation. After centrifugation, cells were resuspended in 5 ml isolation buffer, and incubated with 250 µl sheep anti-rat IgG Dynabeads (Thermo Fisher Scientific) for 30 min at 4°C with tilted rotation. Cells were centrifuged and resuspended in 250 µl of the same Dynabeads for a second 30 min incubation at 4°C with tilted rotation. After each incubation, the tube was placed in a magnet for 2 min, and unbound DN T cells were combined in a new tube. After centrifugation, RNA was extracted from the cell pellet with 1 ml TRIZOL (Ambion) as described below.

Histopathology

Spleen from both control and mutant mice (n=03) was collected and stored in 10% natural buffered formalin (NBF) at 4ºC. The samples were processed for paraffin embedding and longitudinal tissue sections (5 µm) were stained with hematoxylin–eosin (H & E). Stained slides were further scanned by the 3D Histech P250 High-Capacity Slide Scanner in Analytical Imaging Facility of Albert Einstein College of Medicine and analyzed using Case Viewer 2.4 software.

Notch ligand binding assay

Soluble Notch ligands DLL1-Fc (#10184-DL-050), JAG1-Fc (#1277-JG-050), and JAG2-Fc (#1726-JG-050) were purchased from R&D Systems, and DLL4-Fc (#DL4-H5259) was purchased from Acro-biosystems. Single-cell suspensions from thymus were washed in FBB at 4ºC and fixed in PBS-buffered 4% PFA for 15 min at 4ºC. Fixed cells were washed twice with FBB and stored in FBB at 4°C. For analysis, ~0.5-1 x 10^6 fixed thymocytes were washed with FBB and incubated with 40 µl FBB and 1 µl FcR blocking solution (rat-anti-mouse CD16/CD32)

on ice for 15 min. Thereafter, the cells were incubated in 60 µl FBB containing anti-CD4-FITC (1:400), anti-CD8a-PerCp-Cy5.5 (1:400), and 0.75 µg DLL4-Fc, 1.5 µg of DLL1-Fc, JAG1-Fc or JAG2-Fc. After incubation at 4°C for ~30 min, cells were washed with 1 ml FBB and incubated with anti-IgG-APC and anti-IgG-DyLight 405 (Fc-specific) Ab (1:100) at 4°C for 30 min. The cells were then washed with 1 ml FBB and resuspend in 500 µl FBB and analyzed in a flow cytometer (Cytek™, Aurora). For detection of NOTCH1 at the cell surface, fixed thymocytes were incubated with FcR-block rat-anti-mouse CD16/CD32 (1:100) followed by anti-CD4-FITC mAb (1:400), anti-CD8a-PerCp-Cy5.5 (1:400), sheep anti-mouse NOTCH1 Ab (1:50) at 4°C for 30 min, washed, and incubated with rhodamine Red-X-conjugated donkey anti-sheep IgG (1:100) at 4°C for 30 min. Cells were washed with 1 ml FBB, resuspended in 500 µl FBB and analyzed in a FACS flow cytometer (Cytek™, Aurora).

Quantitative RT-PCR

DN T cells from ~$3x10^7$ thymocytes were pipetted vigorously in 1 ml TRIZOL and incubated for 5 min at room temperature before adding 0.2 ml chloroform. Tubes were vortexed for 15s, incubated at room temperature for 2–3 min, and centrifuged at 12,000xg for 15 min at 4°C. The aqueous phase was transferred to a fresh tube, and 0.5 ml isopropanol was added. Samples were incubated at room temperature for 10 min. Following centrifugation at 12,000xg for 10 min at 4°C, the RNA pellet was washed once with 1 ml 75% ethanol. Samples were vortexed and centrifuged at 7500xg for 5 min at 4°C. The RNA pellet was air-dried for 15–20 min and dissolved in 20–50 µl RNase-free water. RNA concentration was determined by Nanodrop and cDNA was prepared from 250 ng RNA using the ReverTra Ace® qPCR RT Master Mix with gDNA Remover (Dc. DiagnoCine) following the manufacturer's protocol. The cDNA was used for quantitative RT-PCR using the primer sequences in table S1.

Statistical analysis

Comparisons are presented as mean ± SEM. Significance was determined by both two-tailed and one-tailed unpaired, parametric, Student t-test analysis (unless otherwise noted) using Prism software version 9.1.

Supplementary Materials

Fig. S1 Gating strategy for BM hematopoietic cell subsets. (Related to Fig. 2, Fig. 5 and fig. S4)

Fig. S2 Gating strategy for thymic immune cell subsets. (Related to Fig. 2, Fig. 6, fig. S4 and S5)

Fig. S3 Gating strategy for splenic immune cell subsets. (Related to Fig. 2, Fig. 7, fig. S4 and fig. S5)

Fig. S4 Immune cell development in *Eogt*[+/+] versus *Eogt*[+/-] mice. (Related to Fig. 2)

Fig. S5 Immune cell subsets from Control versus *Eogt*[-/-] mice. (Related to Fig. 2)

Fig. S6 Gating strategy for BM hematopoietic cell subsets. (Related to Fig. 5)

Fig. S7 Hematopoietic stem progenitors in control, Pof cKO and EPof dKO BM. (Related to Fig. 5)

Fig. S8 Notch ligand binding to Lin-Sca1+ cells. (Related to Fig. 5)

Fig. S9 Thymic immune cell subsets in Pof cKO and EPof dKO mice. (Related to Fig. 6)

Fig. S10 Splenic immune cell subsets in Pof cKO and EPof dKO mice. (Related to Fig. 7)

Table S1 Primer sequences used in genotyping and qRT-PCR

Table S2 Antibodies used in this work

References

1. R. Kopan, Notch Signaling. *Cold Spring Harbor Perspectives in Biology* **4**, a011213-a011213 (2012).
2. R. A. Kovall, B. Gebelein, D. Sprinzak, R. Kopan, The Canonical Notch Signaling Pathway: Structural and Biochemical Insights into Shape, Sugar, and Force. *Dev Cell* **41**, 228-241 (2017).
3. S. Varshney, P. Stanley, Multiple roles for O-glycans in Notch signalling. *FEBS Letters* **592**, 3819-3834 (2018).
4. A. Pandey, N. Niknejad, H. Jafar-Nejad, Multifaceted regulation of Notch signaling by glycosylation. *Glycobiology* **31**, 8-28 (2021).
5. V. C. Luca *et al.*, Structural biology. Structural basis for Notch1 engagement of Delta-like 4. *Science* **347**, 847-853 (2015).
6. V. C. Luca *et al.*, Notch-Jagged complex structure implicates a catch bond in tuning ligand sensitivity. *Science* **355**, 1320-1324 (2017).
7. D. M. Ho, K. G. Guruharsha, S. Artavanis-Tsakonas, The Notch Interactome: Complexity in Signaling Circuitry. *Adv Exp Med Biol* **1066**, 125-140 (2018).
8. F. P. Lampreia, J. G. Carmelo, F. Anjos-Afonso, Notch Signaling in the Regulation of Hematopoietic Stem Cell. *Current Stem Cell Reports* **3**, 202-209 (2017).
9. A. Vanderbeck, I. Maillard, Notch signaling at the crossroads of innate and adaptive immunity. *J Leukoc Biol* **109**, 535-548 (2021).
10. U. Koch *et al.*, Delta-like 4 is the essential, nonredundant ligand for Notch1 during thymic T cell lineage commitment. *J Exp Med* **205**, 2515-2523 (2008).
11. T. B. Feyerabend *et al.*, Deletion of Notch1 Converts Pro-T Cells to Dendritic Cells and Promotes Thymic B Cells by Cell-Extrinsic and Cell-Intrinsic Mechanisms. *Immunity* **30**, 67-79 (2009).
12. M. Romero-Wolf *et al.*, Notch2 complements Notch1 to mediate inductive signaling that initiates early T cell development. *J Cell Biol* **219**, (2020).
13. T. Saito *et al.*, Notch2 is preferentially expressed in mature B cells and indispensable for marginal zone B lineage development. *Immunity* **18**, 675-685 (2003).
14. K. Hozumi *et al.*, Delta-like 1 is necessary for the generation of marginal zone B cells but not T cells in vivo. *Nat Immunol* **5**, 638-644 (2004).

15. K. C. Schröder *et al.*, Adams–Oliver syndrome caused by mutations of the EOGT gene. *Am J Med Genet Part A* **179**, 2246-2251 (2019).
16. J. B. Tan *et al.*, Lunatic and Manic Fringe Cooperatively Enhance Marginal Zone B Cell Precursor Competition for Delta-like 1 in Splenic Endothelial Niches. *Immunity* **30**, 254-263 (2009).
17. B. M. Harvey, R. S. Haltiwanger, Regulation of Notch Function by O-Glycosylation. *Adv Exp Med Biol* **1066**, 59-78 (2018).
18. R. Rampal, K. B. Luther, R. S. Haltiwanger, Notch signaling in normal and disease States: possible therapies related to glycosylation. *Curr Mol Med* **7**, 427-445 (2007).
19. M. Ogawa, T. Okajima, Structure and function of extracellular O-GlcNAc. *Curr Opin Struct Biol* **56**, 72-77 (2019).
20. J. S. Yuan *et al.*, Lunatic Fringe prolongs Delta/Notch-induced self-renewal of committed alphabeta T-cell progenitors. *Blood* **117**, 1184-1195 (2011).
21. I. Visan, J. S. Yuan, Y. Liu, P. Stanley, C. J. Guidos, Lunatic fringe enhances competition for delta-like Notch ligands but does not overcome defective pre-TCR signaling during thymocyte beta-selection in vivo. *J Immunol* **185**, 4609-4617 (2010).
22. I. Visan *et al.*, Regulation of T lymphopoiesis by Notch1 and Lunatic fringe-mediated competition for intrathymic niches. *Nat Immunol* **7**, 634-643 (2006).
23. D. Yao *et al.*, Protein O-fucosyltransferase 1 (Pofut1) regulates lymphoid and myeloid homeostasis through modulation of Notch receptor ligand interactions. *Blood* **117**, 5652-5662 (2011).
24. S. Shi, P. Stanley, Protein O-fucosyltransferase 1 is an essential component of Notch signaling pathways. *Proc Natl Acad Sci* **100**, 5234-5239 (2003).
25. Y. Okamura, Y. Saga, Pofut1 is required for the proper localization of the Notch receptor during mouse development. *Mech Dev* **125**, 663-673 (2008).
26. P. J. Swiatek, C. E. Lindsell, F. F. del Amo, G. Weinmaster, T. Gridley, Notch1 is essential for postimplantation development in mice. *Genes Dev* **8**, 707-719 (1994).
27. R. A. Conlon, A. G. Reaume, J. Rossant, Notch1 is required for the coordinate segmentation of somites. *Development* **121**, 1533-1545 (1995).
28. C. Oka *et al.*, Disruption of the mouse RBP-J kappa gene results in early embryonic death. *Development* **121**, 3291-3301 (1995).
29. V. W. C. Yu *et al.*, Specific bone cells produce DLL4 to generate thymus-seeding progenitors from bone marrow. *J Exp Med* **212**, 759-774 (2015).
30. K. Matsumoto *et al.*, Dual Roles of O-Glucose Glycans Redundant with Monosaccharide O-Fucose on Notch in Notch Trafficking. *J Biol Chem* **291**, 13743-13752 (2016).
31. H. Takeuchi *et al.*, O-Glycosylation modulates the stability of epidermal growth factor-like repeats and thereby regulates Notch trafficking. *J Biol Chem* **292**, 15964-15973 (2017).
32. Y. Wang *et al.*, Uncontrolled angiogenic precursor expansion causes coronary artery anomalies in mice lacking Pofut1. *Nat Commun* **8**, 578 (2017).
33. A. Matsuura *et al.*, O-linked N-acetylglucosamine is present on the extracellular domain of notch receptors. *J Biol Chem* **283**, 35486-35495 (2008).
34. Y. Sakaidani *et al.*, O-linked-N-acetylglucosamine on extracellular protein domains mediates epithelial cell-matrix interactions. *Nat Commun* **2**, 583 (2011).

35. R. Müller, A. Jenny, P. Stanley, The EGF Repeat-Specific O-GlcNAc-Transferase Eogt Interacts with Notch Signaling and Pyrimidine Metabolism Pathways in Drosophila. *PLoS ONE* **8**, e62835 (2013).
36. S. Sawaguchi *et al.*, O-GlcNAc on NOTCH1 EGF repeats regulates ligand-induced Notch signaling and vascular development in mammals. *eLife* **6**, (2017).
37. Y. Song, V. Kumar, H.-X. Wei, J. Qiu, P. Stanley, Lunatic, manic, and radical fringe each promote T and B cell development. *J Immunol* **196**, 232-243 (2016).
38. P. Stanley, V. Kumar, A. Tanwar, Roles of Notch Glycoslation in Signaling. *The FASEB Journal* **35**, (2021).
39. L. Atzmony, T. D. Zaki, R. J. Antaya, K. A. Choate, Phenotypic expansion of POFUT1 loss of function mutations in a disorder featuring segmental dyspigmentation with eczematous and folliculo-centric lesions. *Am J Med Genet A* **179**, 2469-2473 (2019).
40. K. Hozumi *et al.*, Delta-like 4 is indispensable in thymic environment specific for T cell development. *J Exp Med* **205**, 2507-2513 (2008).
41. P. Stanley, C. J. Guidos, Regulation of Notch signaling during T- and B-cell development byO-fucose glycans. *Immunological Reviews* **230**, 201-215 (2009).
42. R. Lakhan, C. V. Rathinam, Deficiency of Rbpj Leads to Defective Stress-Induced Hematopoietic Stem Cell Functions and Hif Mediated Activation of Non-canonical Notch Signaling Pathways. *Front Cell Dev Biol* **8**, (2021).
43. A. Tanwar, P. Stanley, Regulation of Notch Signaling By O-Glycans during Lymphopoiesis and Myelopoiesis. *Blood* **138**, 2170-2170 (2021).
44. E. M. Pietras *et al.*, Functionally Distinct Subsets of Lineage-Biased Multipotent Progenitors Control Blood Production in Normal and Regenerative Conditions. *Cell Stem Cell* **17**, 35-46 (2015).
45. E. L. Y. Chen, P. K. Thompson, J. C. Zúñiga-Pflücker, RBPJ-dependent Notch signaling initiates the T cell program in a subset of thymus-seeding progenitors. *Nat Immunol* **20**, 1456-1468 (2019).
46. T. S. Heng, M. W. Painter, C. Immunological Genome Project, The Immunological Genome Project: networks of gene expression in immune cells. *Nat Immunol* **9**, 1091-1094 (2008).

Acknowledgments: We thank Dr. Jinghang Zhang and Aodengtuya of the Flow Cytometry Core Facility of the Albert Einstein Cancer Center for their assistance in discussing multi-color flow cytometry experimental strategies. We are also thankful to Subha Sundaram for her technical support and Swathi-Rao Narayanagari for her assistance in the bone marrow transplantation (BMT) study. We also thank Hillary Guzik and Andrea Briceno from the Analytical Imaging Facility of the Einstein Cancer Center for slide scanning using a 3D Histech P250 High-Capacity Slide Scanner purchased with NIH SIG #1S10OD019961-01.

Funding: This work was supported by

National Institutes of Health grant RO1 GM-106417 (PS)

National Institutes of Health grant PO1 grant CA-13330 (partial support from core facilities)

Author contributions:

Conceptualization: PS

Methodology: PS, AT

Investigation: AT, PS

Visualization: AT, PS

Funding acquisition: PS

Project administration: PS

Supervision: PS

Writing – original draft: AT

Writing – review & editing: PS, AT

Competing interests: Authors declare that they have no competing interests.

Data and materials availability: All data are available in the main text or the supplementary materials.

Figures:

Fig. 1. **Expression of *Eogt* and *Pofut1* in immune cell subsets** The diagram depicts the ECD of mouse NOTCH1 showing the 36 EGF repeats and the O-glycans attached at respective consensus sites. The sugar that initiates each O-glycan is shown. The potential extensions of O-fucose and O-GlcNAc glycans are also shown. The expression of *Eogt* and *Pofut1* in immune cells is from ImmGen Gene Skyline ULI RNASeq data group for *Eogt* and *Pofut1* gene expression (*46*) http://rstats.immgen.org/Skyline/skyline.html).

Fig. 2. Altered lymphoid and myeloid subsets in mice lacking *Eogt* and O-GlcNAc glycans

(**A**) Absolute cell numbers or frequency (%) for lymphoid and myeloid cell subsets in bone marrow that differed between Control (*Eogt*[+/+] and *Eogt*[+/-]) and *Eogt*[-/-] mice. See fig. S1 for gating, fig. S4 for data of *Eogt*[+/+] versus *Eogt*[+/-] and fig. S5 for BM cellularity. (**B**) Absolute cell numbers or frequency (%) for lymphoid and myeloid cell subsets in thymus that differed between Control (*Eogt*[+/+] and *Eogt*[+/-]) and *Eogt*[-/-] mice. See fig. S2 for gating, fig. S4 for data of *Eogt*[+/+] versus *Eogt*[+/-] and fig. S5 for subsets that did not differ significantly. (**C**) Absolute cell numbers or frequency (%) for lymphoid and myeloid cell subsets in spleen that differed between Control (*Eogt*[+/+] and *Eogt*[+/-]) and *Eogt*[-/-] mice. See fig. S3 for gating, fig. S4 for data of *Eogt*[+/+] versus *Eogt*[+/-] and fig. S5 for subsets that did not differ significantly. Each symbol represents a mouse of 7-8 weeks. Data are presented as mean ± SEM. *$p < 0.05$, **$p<0.01$,***$p<0.001$, ****$p<0.0001$ based on two-tailed Student t test and (*) $p < 0.05$ based on one-tailed Student t test.

Fig. 3. The *Eogt* null phenotype is largely cell autonomous

Bone marrow cells ($3X10^6$) from *Eogt*[+/-] or *Eogt*[-/-] mice expressing CD45.2 were injected via the retro-orbital plexus into lethally-irradiated, wild-type recipient males expressing CD45.1. Recipient BM, thymus and spleen were analyzed 7 weeks after transplantation. (**A**) Flow cytometry profile and histograms of bone marrow from recipient mice (CD45.1+) that received BM from *Eogt*[+/-] or *Eogt*[-/-] mice. The approximate donor contribution was 78% for *Eogt*[+/-] and 57% for *Eogt*[-/-] of recipient BM. (**B**) Absolute cell number and frequency (%) of B cells and dendritic cells in bone marrow that differed when transferred from *Eogt*[+/-] versus *Eogt*[-/-] donor bone marrow. (**C**) Absolute cell number and frequency (%) of T cell progenitors in thymus that differed when derived from *Eogt*[+/-] versus *Eogt*[-/-] donor bone marrow. (**D**) Absolute cell number and frequency (%) of B cells and granulocyte subsets in spleen that differed when derived from *Eogt*[+/-] versus *Eogt*[-/-] donor bone marrow. Each symbol represents a mouse of 7-8 weeks. Data are presented as mean ± SEM. *p <0.05, **p<0.01 based on two-tailed Student t test. (*) p <0.05 based on one-tailed Student t test.

Fig. 4. Notch signalling in *Eogt* null T cell progenitors

Representative flow cytometry profiles and histogram quantification of (**A**) Cell surface expression of NOTCH1, binding of DLL1-Fc, DLL4-Fc, JAG1-Fc and JAG2-FC to fixed CD4/CD8 DN T cell progenitors from *Eogt*[+/-] or *Eogt*[-/-] mice. Mean fluorescence index (MFI) for anti-Fc Ab was subtracted from MFI for Notch ligand or NOTCH1 (MFI-control). Symbols represent *Eogt*[+/-] (blue circles) and *Eogt*[-/-] (red circles) DN T cells. Fixed cells had been stored for up to 3 months at 4°C. (**B**) Transcripts from DN T cell progenitors of *Eogt*[+/-] or *Eogt*[-/-] mice were subjected to qRT-PCR as described in Materials and Methods. Relative expression was determined based on the average delta Ct obtained for *Gapdh* and *Hprt* combined. Each symbol represents a mouse of 7-8 weeks. Data are presented as mean ± SEM. *p <0.05, **p<0.01 based on two-tailed Student t test and (*) p <0.05 based on one-tailed Student t test.

Fig. 5. Hematopoiesis in EPof dKO bone marrow

Hematopoiesis was analyzed in bone marrow of *Eogt*[+/-]*Pofut1*[F/F] (Control), *Pofut1*[F/F]:*Vav1-iCre* (Pof cKO) and *Eogt*[-/-]*Pofut1*[F/F]*:Vav1-iCre* (EPof dKO) mice. Absolute numbers or frequency (%) of hemopoietic cell subsets in bone marrow are shown. Gating strategies are shown in fig. S6 and additional data are shown in fig. S7. Short term-hemopoietic stem cells (ST-HSC), long-term hemopoietic stem cell (LT-HSC), Lin-Sca1+c-Kit+ (LSK) cells, hematopoietic stem progenitor cells (HSPCs), multipotent progenitor-2, -3, -4 (MPP2, -3, -4), lymphoid primed multipotent progenitor cell (LMPP), common lymphoid progenitor (CLP), common myeloid progenitor (CMP), granulocyte monocyte progenitor (GMP), megakaryocyte erythrocyte progenitor (MEP), T cells, B cells and myeloid cells. Each symbol represents a mouse of 7-8 weeks. Data

are presented as mean ± SEM. *p <0.05, **p<0.01, ***p<0.001, ****p<0.001 based on two-tailed Student t test and (*) p <0.05 based on one-tailed Student t test.

Fig. 6. Impaired T cell development in Pof cKO thymus is worse in EPof dKO thymus

(**A**) Thymus weight compared to body weight. (**B**) Representative flow cytometry profiles of thymocytes using Abs to CD4 versus CD8 cell surface markers after gating on live cells. (**C**) Absolute cell numbers or frequency (%) of T cell subsets that differed between Control and either mutant. ETP (DN1 cells that were cKit/CD117+), DN1 (CD44+CD25-), DN2 (CD44+CD25+), DN3 (CD44-CD25+), and DN4 (CD44-CD25-) T cell progenitors, DN (CD4 and CD8 double negative), DP (CD4 and CD8 double positive). **(D)** Absolute cell numbers or frequency (%) of B cell and myeloid cell subsets that differ from control are shown. Additional data are shown in fig. S9. Each symbol represents a mouse of 7-8 weeks. Data are presented as mean ± SEM. *p <0.05, **p<0.01, ***p<0.001, ****p<0.001 based on two-tailed Student t test and (*) p <0.05 based on one-tailed Student t test.

Fig. 7. Impaired B cell development in Pof cKO spleen is worse in EPof dKO spleen

(**A**) Splenomegaly and extramedullary hematopoiesis. (**B**) Spleen weight compared to body weight. (**C**) Flow cytometric profiles and histogram quantification for CD4 versus CD8 cell surface expression after gating on live cells. (**D**) Absolute cell numbers or frequency (%) of splenic lymphoid and myeloid cell subsets that differed from control are shown. Fo-B (follicular B cells), MZ-B (marginal zone-B), MZ-P (marginal zone precursor), dendritic cells (CD11b/c), natural killer T cells (NK1.1) and granulocytes (Gr-1). Additional data are shown in fig. S10. Each symbol represents a mouse of 7-8 weeks. Data are presented as mean ± SEM. *p <0.05, **p<0.01, ***p<0.001, ****p<0.001 based on two-tailed Student t test and (*) p <0.05, based on one-tailed Student t test.

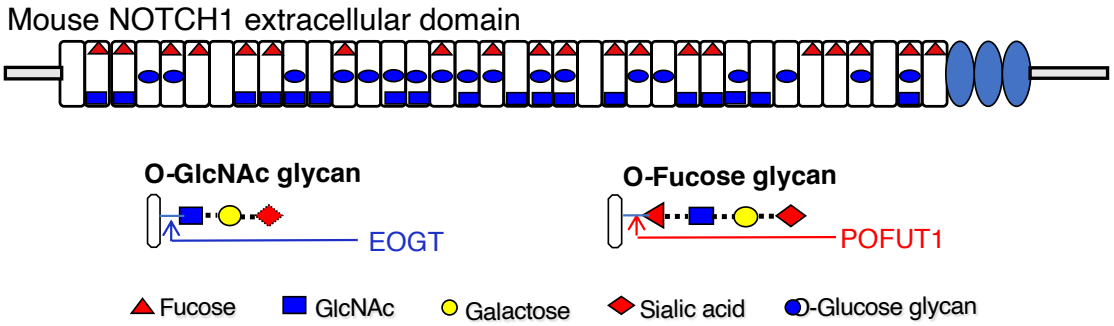

Eogt

Expression value normalized by DESeq2

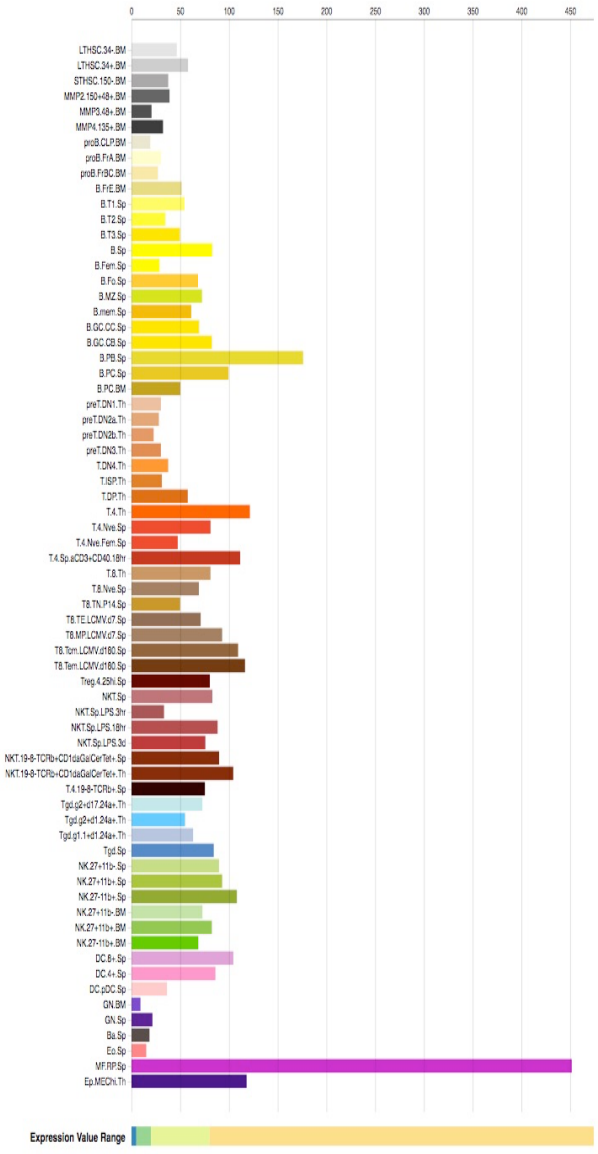

Pofut1

Expression value normalized by DESeq2

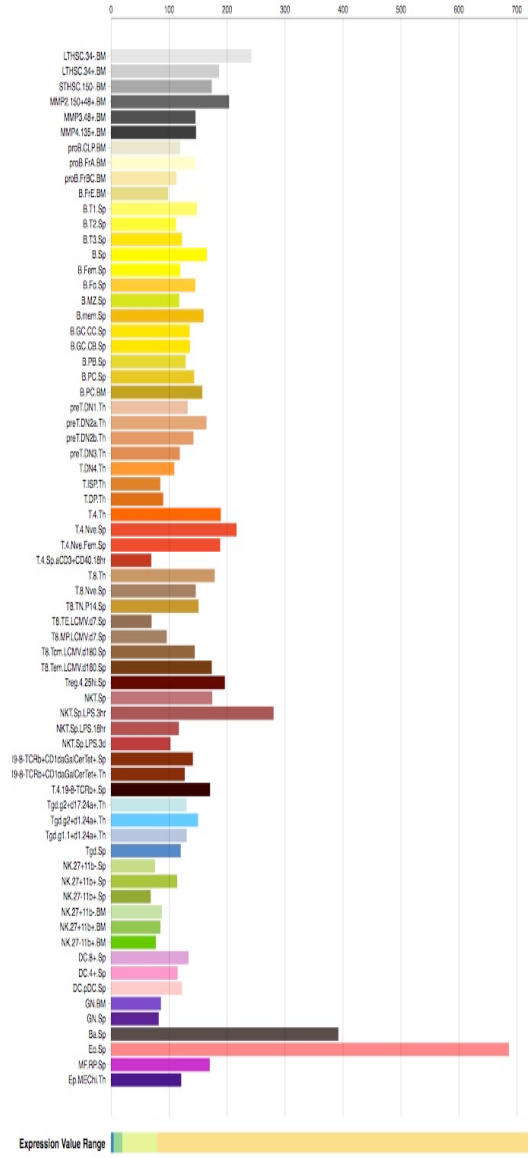

A Bone Marrow

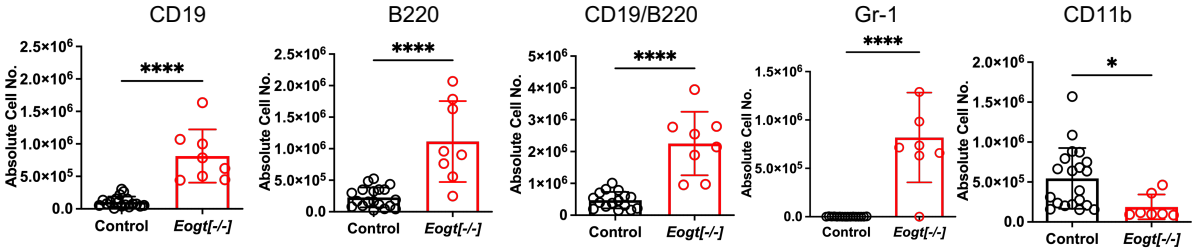

B Thymus

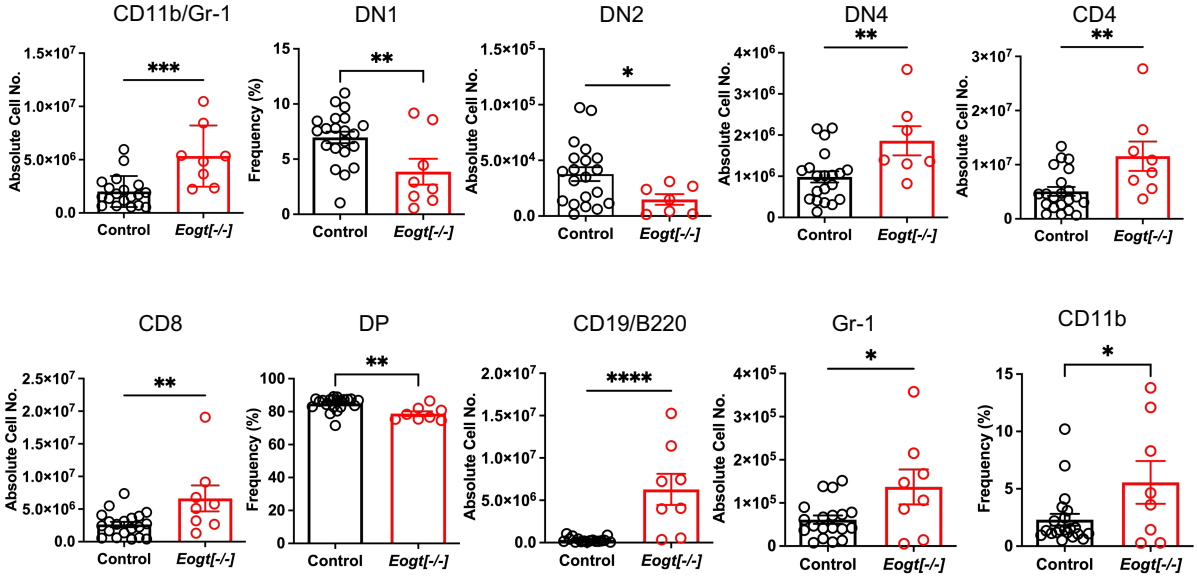

C Spleen

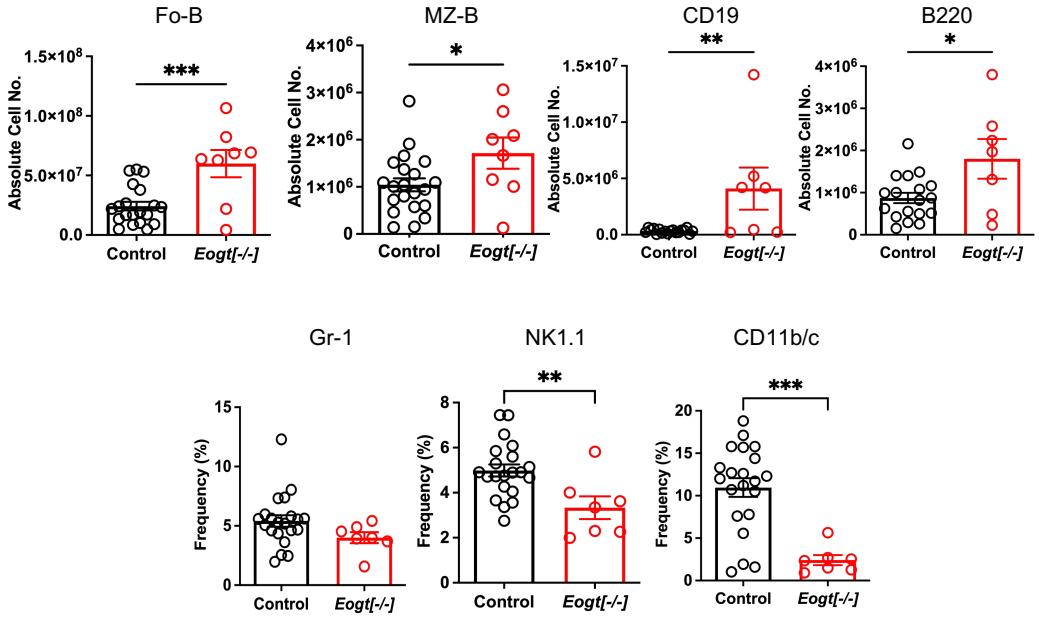

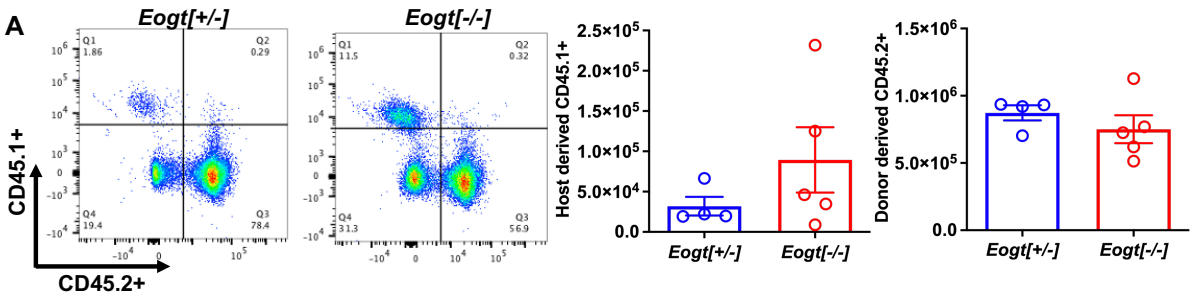

B Bone Marrow

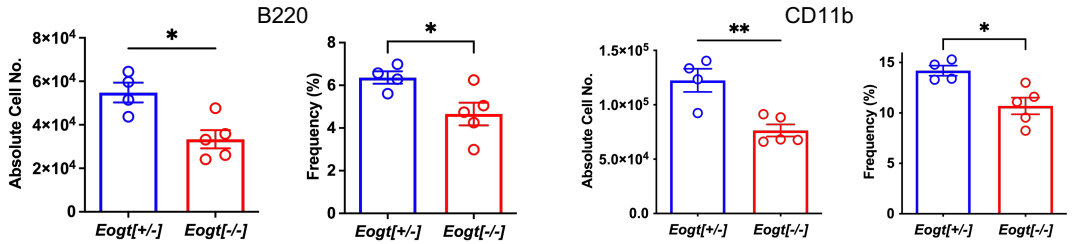

C Thymus

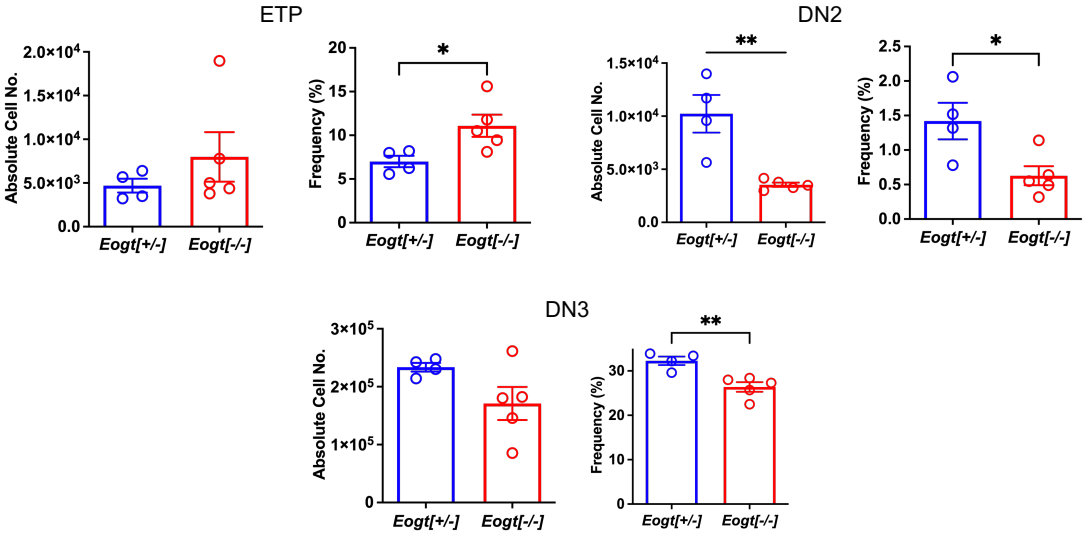

D Spleen

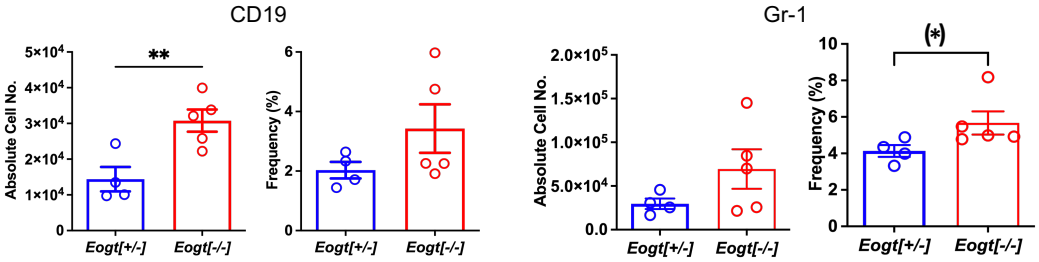

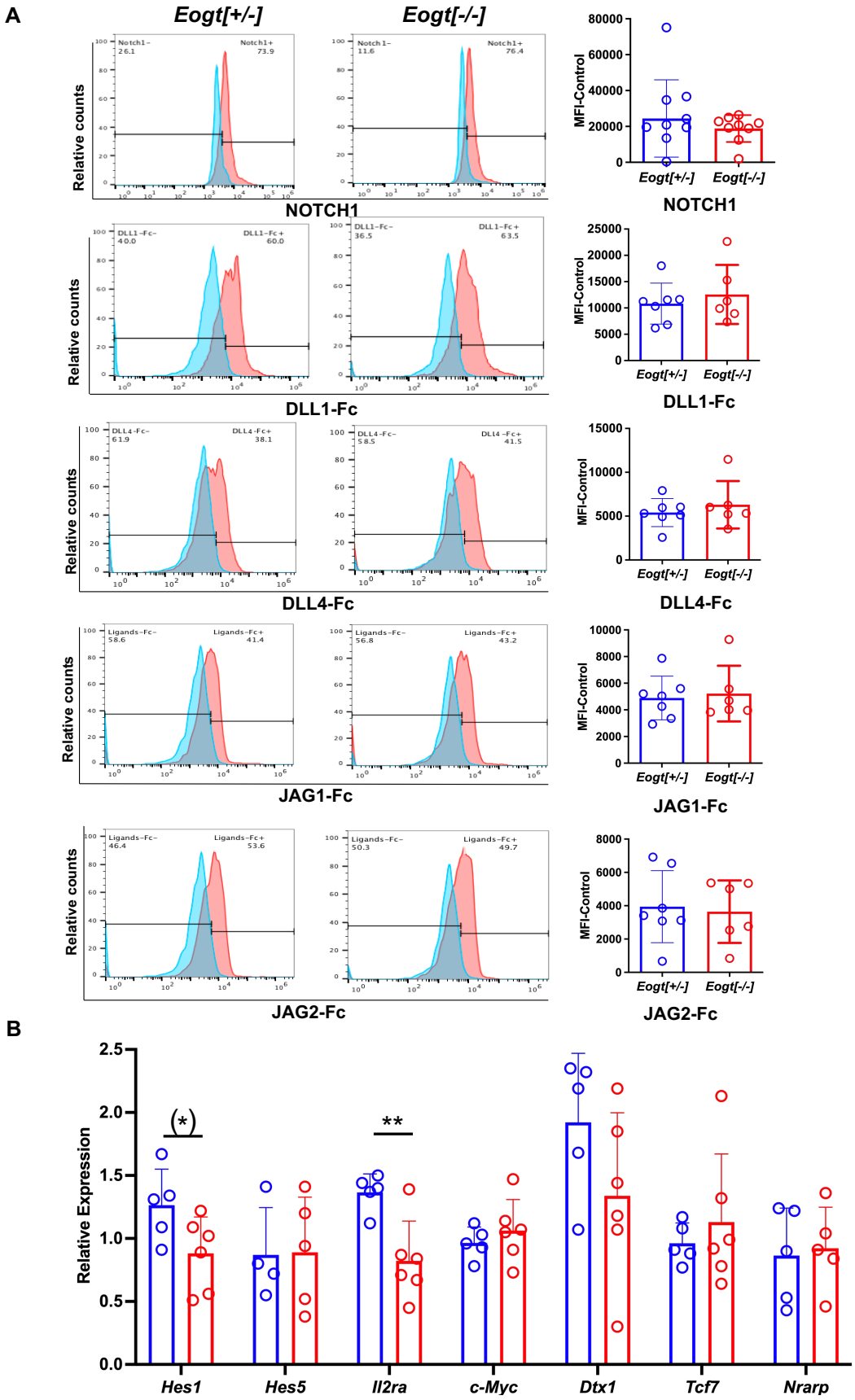
A
Eogt[+/-]
Eogt[-/-]
Relative counts
Notch1- 26.1
Notch1+ 73.9
Notch1- 11.6
Notch1+ 76.4
NOTCH1
MFI-Control
DLL1-Fc- 40.0
DLL1-Fc+ 60.0
DLL1-Fc- 36.5
DLL1-Fc+ 63.5
DLL1-Fc
DLL4-Fc- 61.9
DLL4-Fc+ 38.1
DLL4-Fc- 58.5
DLL4-Fc+ 41.5
DLL4-Fc
Ligands-Fc- 58.6
Ligands-Fc+ 41.4
Ligands-Fc- 56.8
Ligands-Fc+ 43.2
JAG1-Fc
Ligands-Fc- 46.4
Ligands-Fc+ 53.6
Ligands-Fc- 50.3
Ligands-Fc+ 49.7
JAG2-Fc
B
Relative Expression
(*)
**
Hes1
Hes5
Il2ra
c-Myc
Dtx1
Tcf7
Nrarp

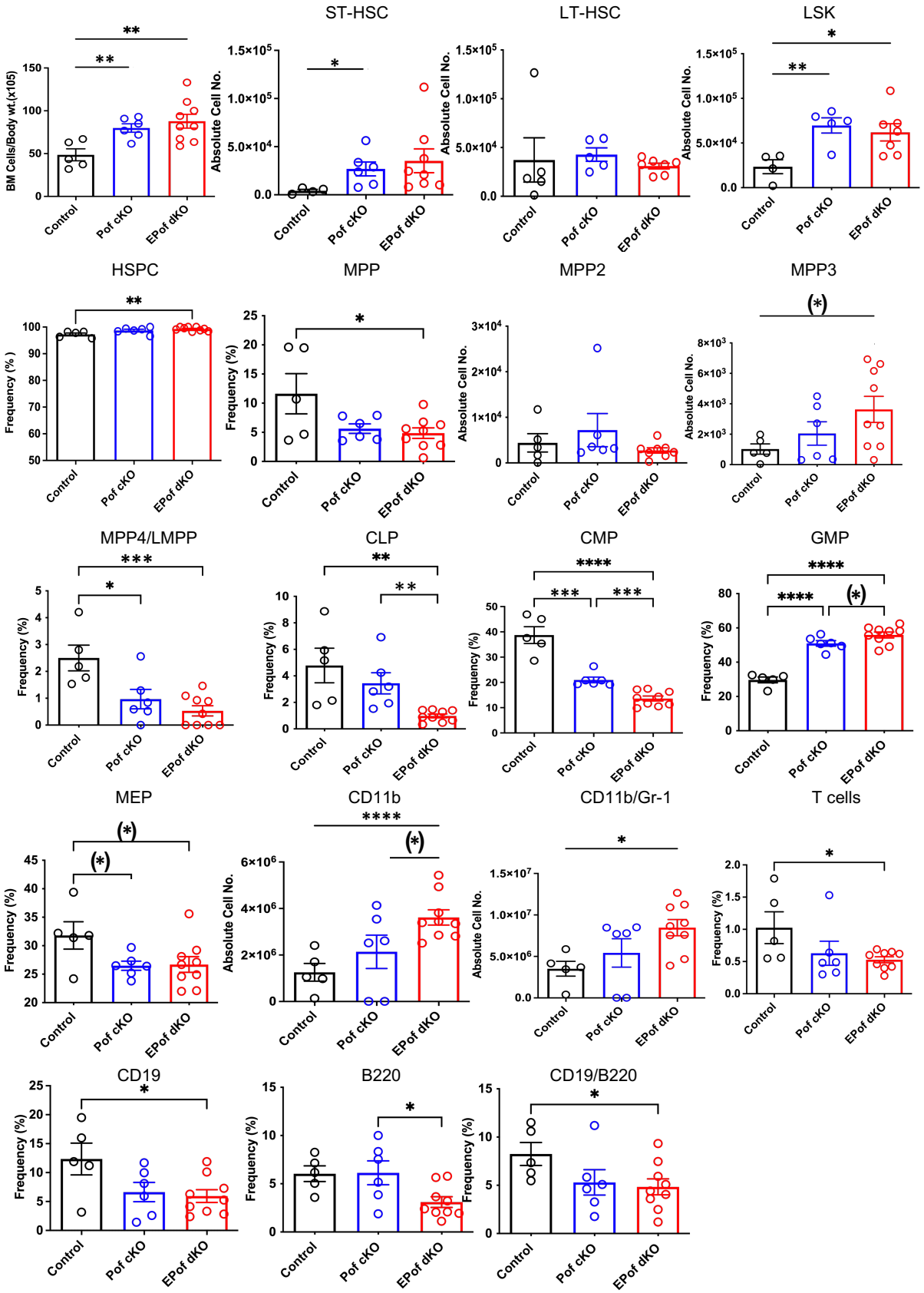
BM Cells/Body wt.(x105)
ST-HSC
LT-HSC
LSK
HSPC
MPP
MPP2
MPP3
MPP4/LMPP
CLP
CMP
GMP
MEP
CD11b
CD11b/Gr-1
T cells
CD19
B220
CD19/B220
Frequency (%)
Absolute Cell No.
Control
Pof cKO
EPof dKO

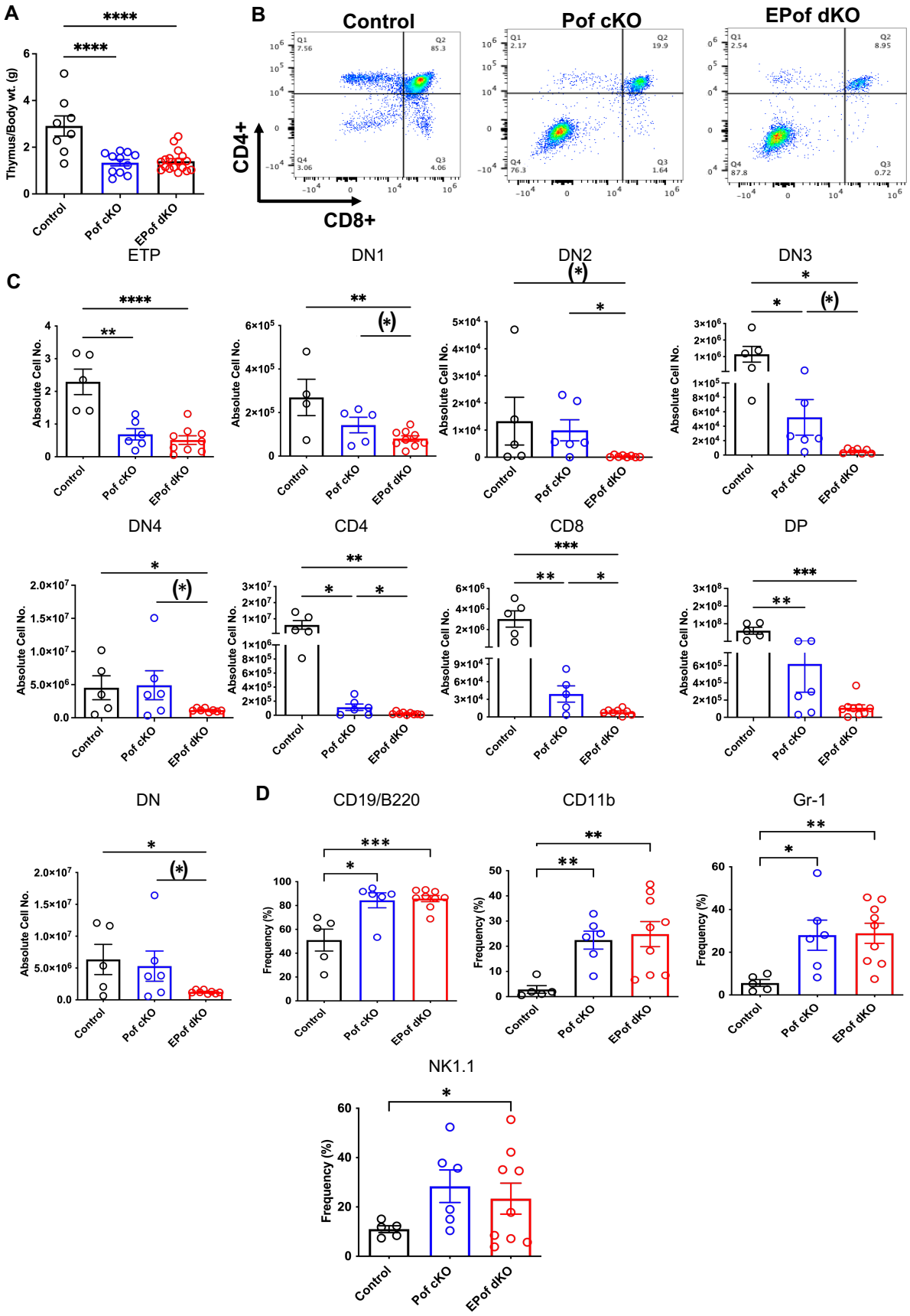
A
Thymus/Body wt. (g)
Control
Pof cKO
EPof dKO
B
Control
Pof cKO
EPof dKO
CD4+
CD8+
C
ETP
DN1
DN2
DN3
DN4
CD4
CD8
DP
DN
Absolute Cell No.
D
CD19/B220
CD11b
Gr-1
NK1.1
Frequency (%)

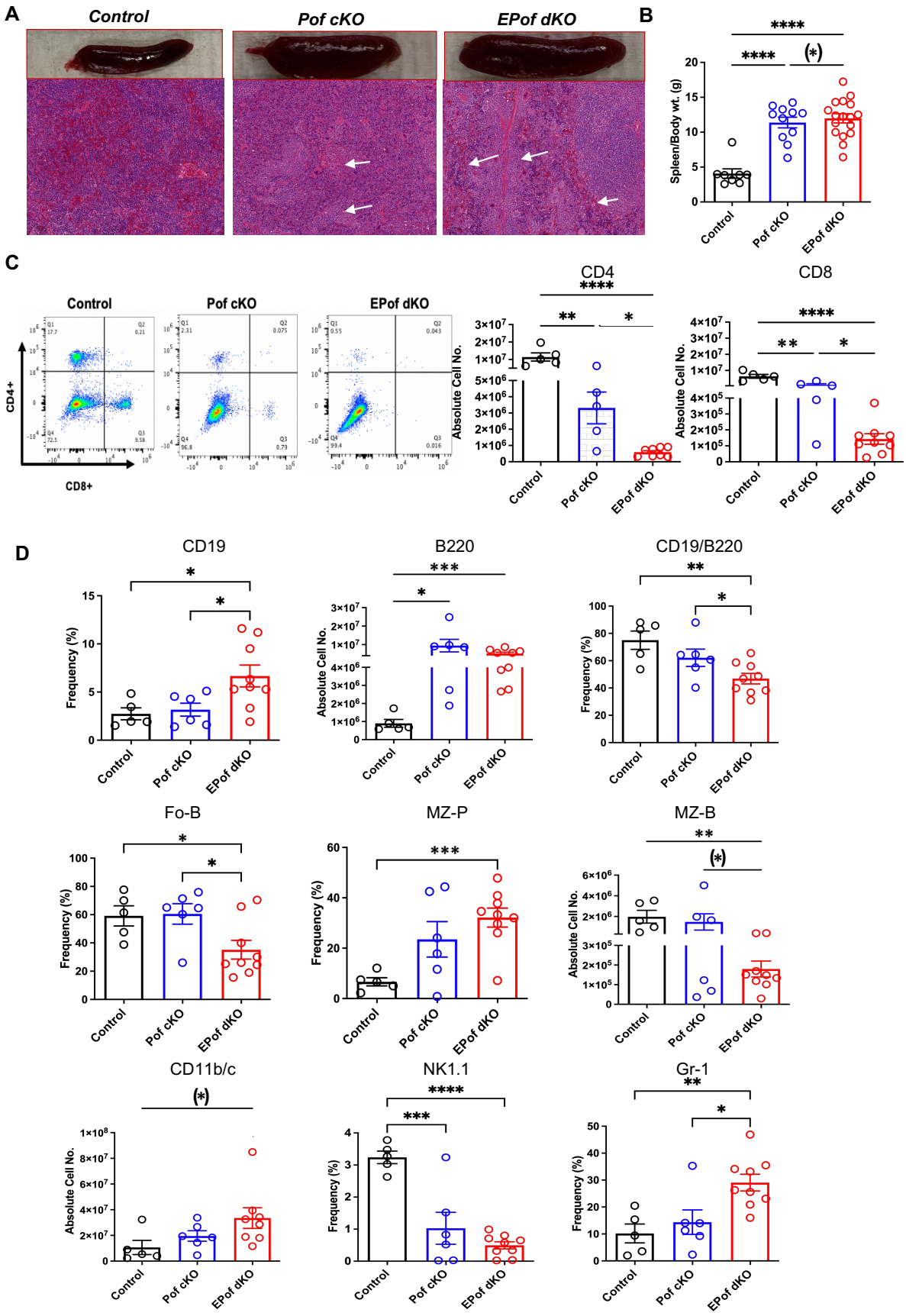
A
Control
Pof cKO
EPof dKO
B
Spleen/Body wt. (g)
Control
Pof cKO
EPof dKO
C
Control
Pof cKO
EPof dKO
CD4+
CD8+
CD4
CD8
Absolute Cell No.
D
CD19
B220
CD19/B220
Fo-B
MZ-P
MZ-B
CD11b/c
NK1.1
Gr-1
Frequency (%)
Absolute Cell No.

Synergistic Regulation of Notch Signaling by Different O-Glycans Promotes Hematopoiesis

Ankit Tanwar,[1] Pamela Stanley[1]*

[1]Dept. Cell Biology, Albert Einstein College of Medicine, New York, NY, USA

*Corresponding author. Email: pamela.stanley@einsteinmed.edu

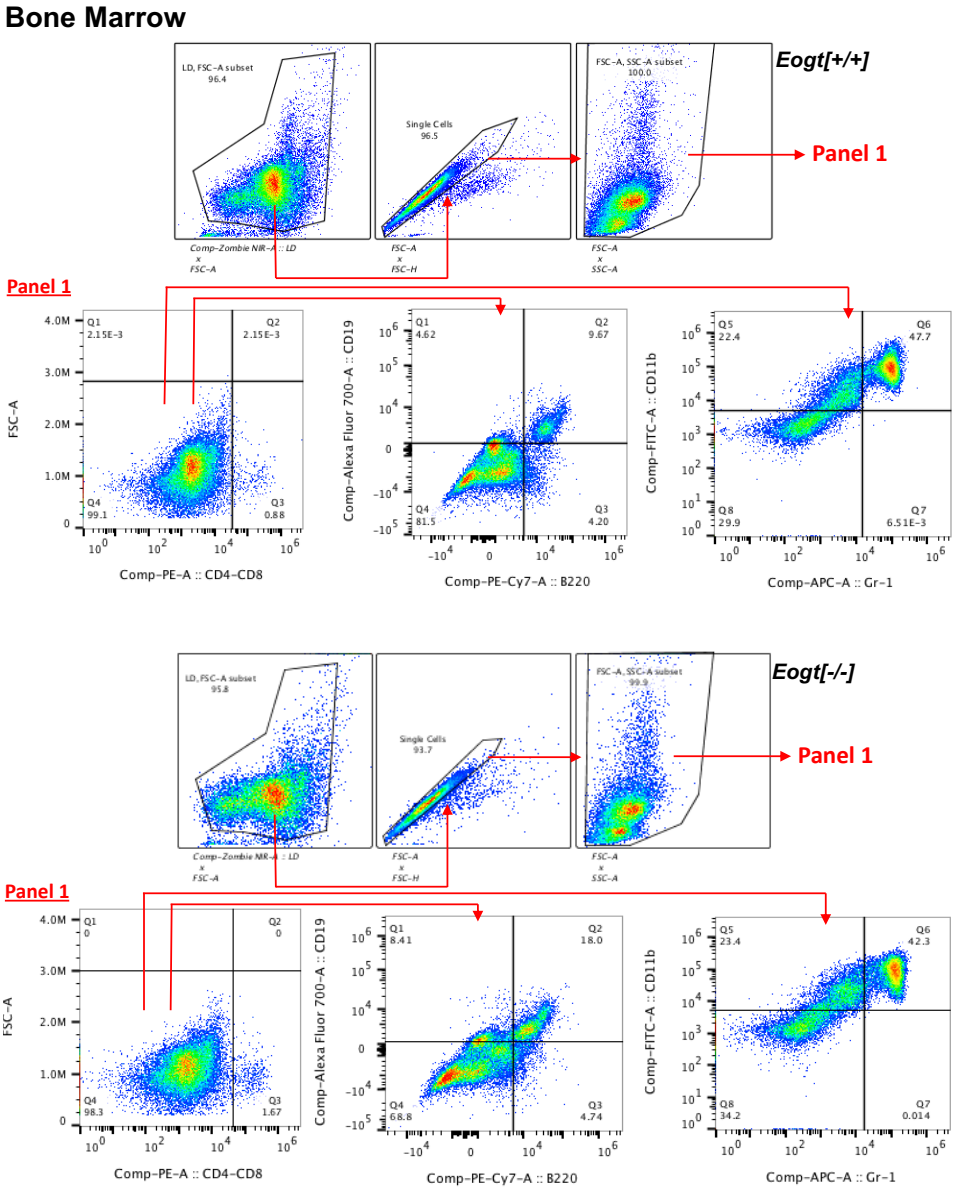

Fig. S1 Gating strategy for BM immune cell subsets. (Related to Fig. 2, Fig. 5, and fig. S4)

Flow cytometry profiles of BM cells from a 7-8 week old *Eogt*[+/+] or *Eogt*[-/-] mouse selected after gating on live cells using Zombie NIR dye in the Cytek™ Aurora flow cytometer. Live singlets were selected (FSC-H vs FSC-A) and the main population (SSC-A vs FSC-A) was plotted for CD4+CD8+ vs FSC-A, and gated on CD4-CD8- cells to compare CD19+ vs B220+ or CD11b+ vs Gr-1+ cell populations.

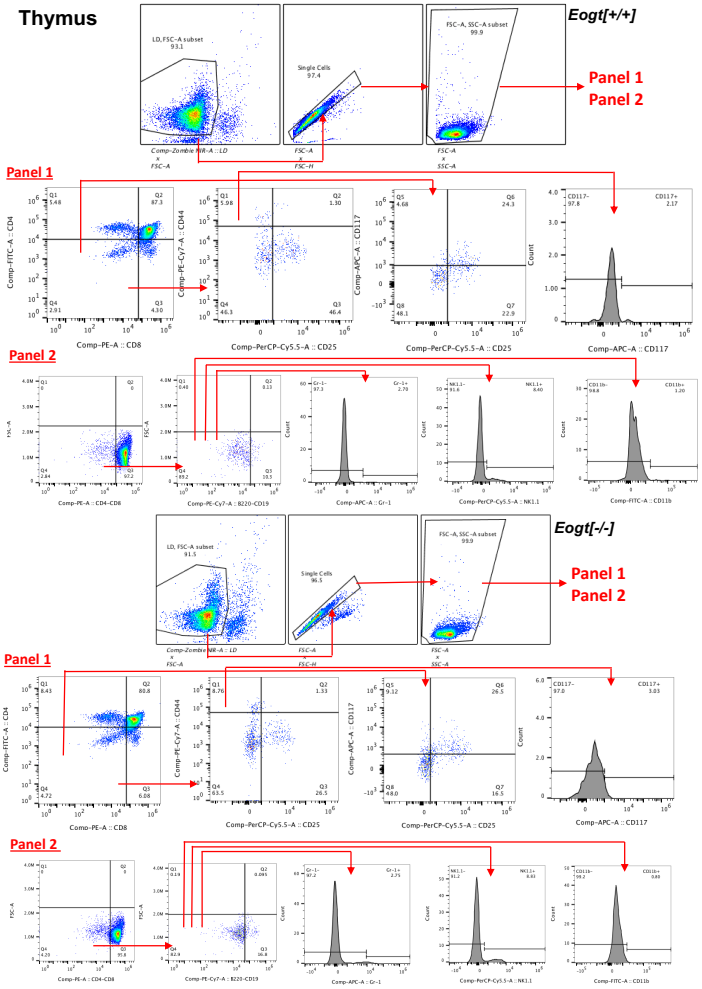

Fig. S2 Gating strategy for thymic immune cell subsets. (Related to Fig. 2, Fig. 6, fig. S4 and fig. S5)

Flow cytometry profiles of thymocytes from a 7-8 week old *Eogt*[+/+] or *Eogt*[-/-] mouse selected after gating on live cells using Zombie NIR dye in the Cytek™ Aurora flow cytometer. Live singlets were selected (FSC-H vs FSC-A) and the main population (SSC-A vs FSC-A) was plotted for Panel 1 antibodies to CD4 vs CD8 to determine frequencies and absolute numbers of CD4+ SP and CD8+ SP T cells, CD4+CD8+ DP T cells and CD4-CD8- DN T cells. The DN T cell population was plotted for CD44 vs CD25 to determine frequencies and absolute numbers of CD44+CD25- (DN1), CD44+CD25+ (DN2), CD44-CD25+ (DN3) and CD44-CD25- (DN4) T cell progenitors, and CD117+ DN1 cells (ETP). Panel 2 antibodies were used to plot FSC-A vs CD4/CD8 to gate on CD4-CD8- cells to then determine frequencies and absolute numbers of non-T cells in the thymus by plotting CD19 vs B220, and gating on CD19-B220- to determine non-B Gr-1+, NK1.1+, CD11b+ cells. Flow cytometry plots show B cells (B220+/CD19+), myeloid cells (CD11b+), granulocytes (Gr-1+), and natural killer T-cells (NK1.1+).

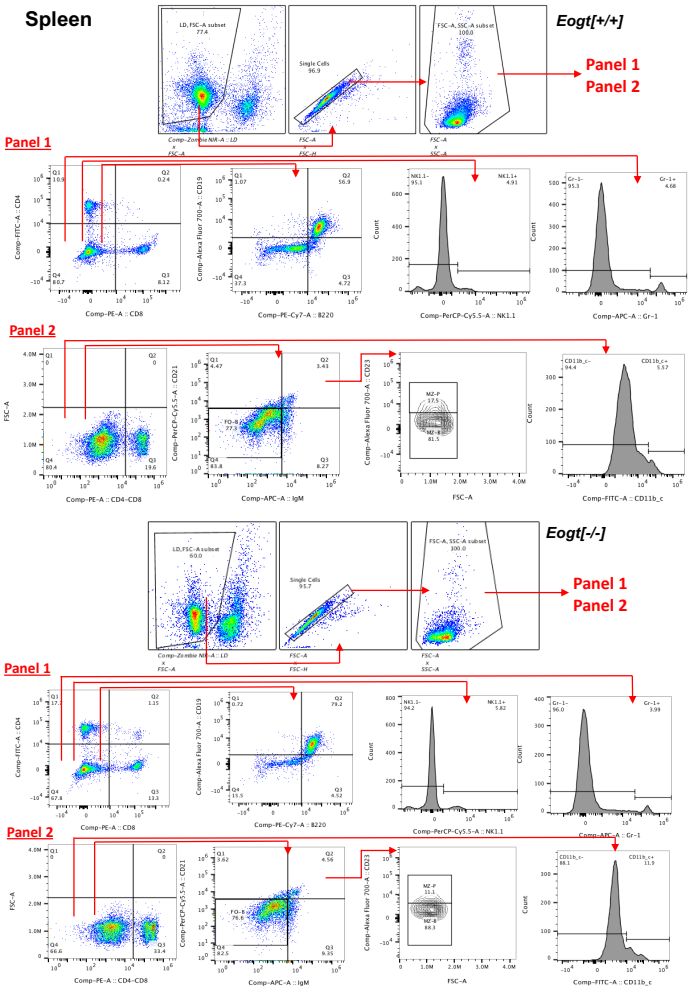

Fig. S3 Gating strategy for splenic immune cell subsets. (Related to Fig. 2, Fig. 7, Fig. S4 and Fig. S5)

Flow cytometry profiles of splenocytes from a 7-8 week old *Eogt*[+/+] or *Eogt*[-/-] mouse selected after gating on live cells using Zombie NIR dye in the Cytek™ Aurora flow cytometer. Live singlets were selected (FSC-H vs FSC-A) and the main population (SSC-A vs FSC-A) was used with Panel 1 antibodies to plot CD4 vs CD8**;** non-T cells (CD4-CD8-) were used to plot CD19 vs B220 to determine frequencies and absolute numbers of B cells, natural killer T cells (NK1.1), or granulocytes (Gr-1)**.** Panel 2 antibodies were used with the main population of singlets to plot FSC-A vs CD4/CD8**;** non-T cells (CD4-/CD8-) were used to plot CD21 vs IgM or CD11b/c**;** CD21+IgM+ were used to plot CD23+ vs FSC-A. Flow cytometric profiles show Fo-B cells (IgM $^{int/lo}$ CD21+) and histogram showing CD11b. The IgM+CD21+ subset was further subdivided into MZ-P and MZ-B cells based on forward scatter and CD23 expression.

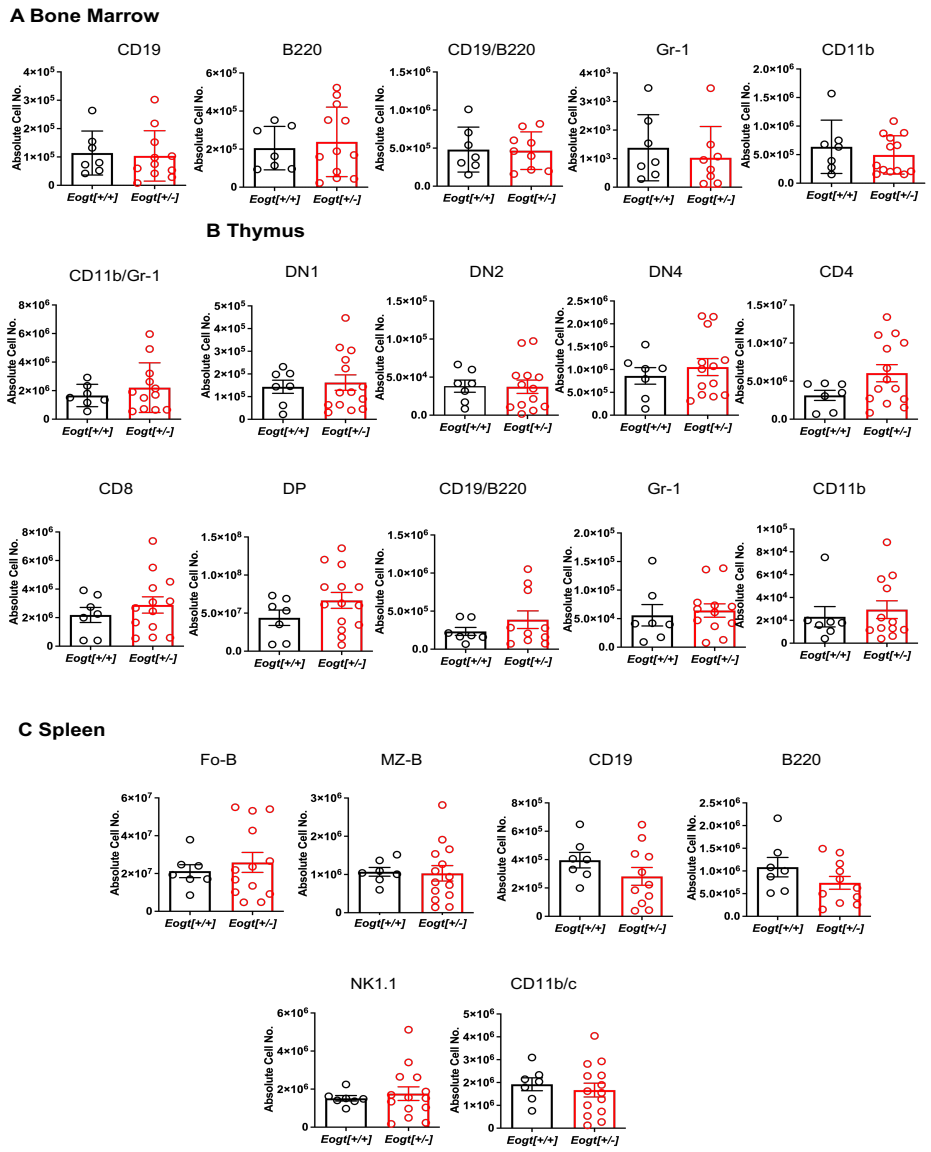

Fig. S4 Immune cell development in *Eogt* [+/+] and *Eogt*[+/-]. (Related to Fig. 2)

(**A**) Absolute cell numbers of CD19+ B220+ B cells, myeloid cells (CD11b+), and granulocytes (Gr-1+) in bone marrow. (**B**) Absolute cell numbers of CD44+CD25- (DN1), CD44+CD25+ (DN2), and CD44-CD25- (DN4) T cell progenitors, CD4+ SP, CD8+ SP, CD4+CD8+ DP T cells and B cells (B220+/CD19+), granulocytes (Gr-1+) and myeloid cells (CD11b+) in thymus. (**C**) Absolute numbers of follicular-B (Fo-B), marginal zone B (MZ-B), CD19+, B220+ B cells, natural killer T cells (NK1.1+), and dendritic cells (CD11b/c+). Each symbol represents a mouse 7-8 weeks.

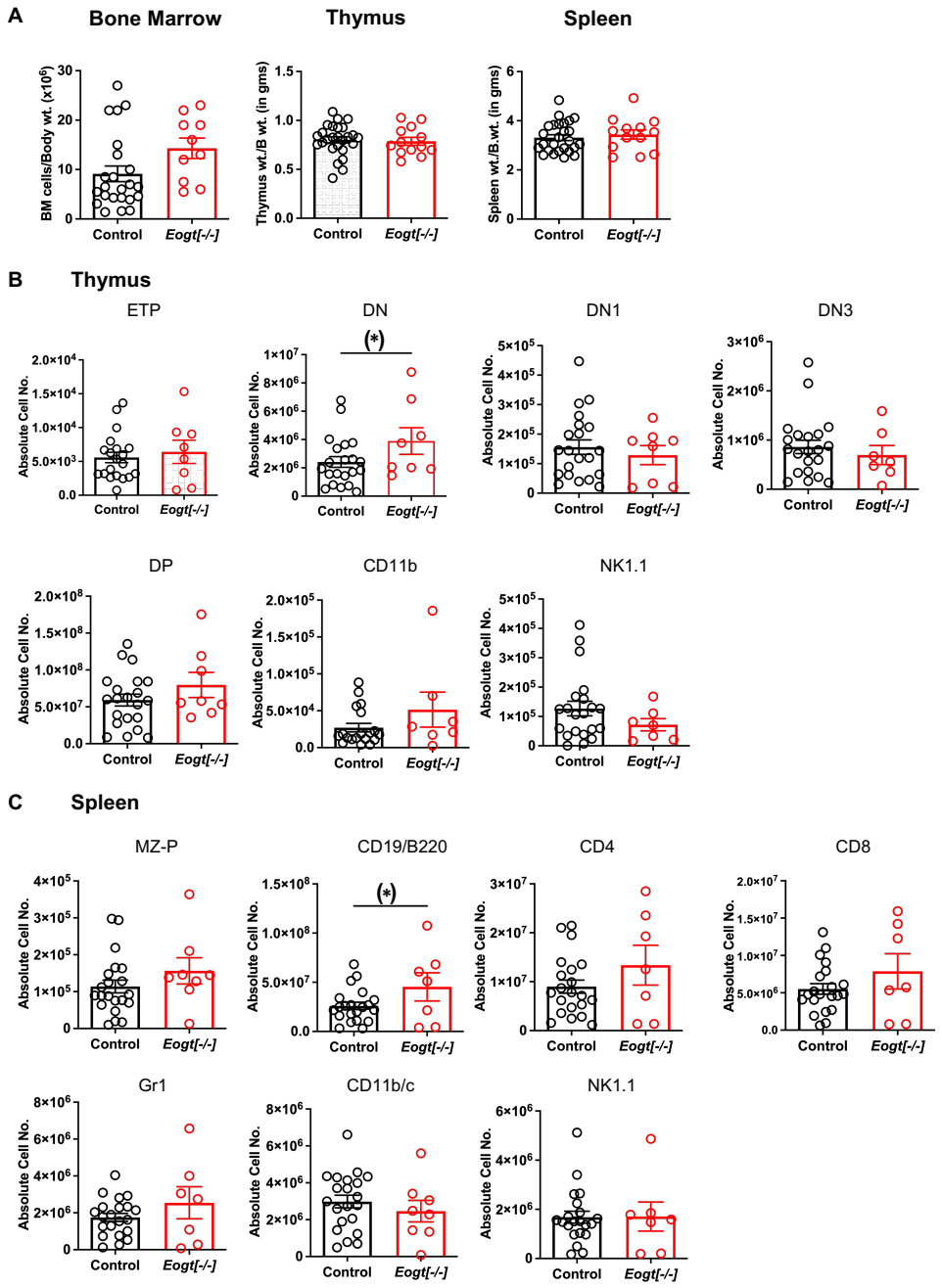

Fig. S5 Immune cell subsets in Control versus *Eogt*[-/-] mice. (Related to Fig. 2)

(**A**) Bone Marrow cellularity, thymus to body weight and spleen to body weight. (**B**) Absolute cell numbers of ETP, DN, DN1, DN3, DP, myeloid cells (CD11b+) and natural killer T cells (NK1.1+) in thymus. (**C**) Absolute cell numbers MZ-B, B cells (CD19+/B220+), CD4+, CD8+ T cells, granulocytes (Gr-1+), dendritic cells (CD11b/c), and natural killer T cells (NK1.1) in spleen. Each symbol represents a mouse 7-8 weeks. Data presented as mean SEM. (*) $p < 0.05$ based on one-tailed Student t test.

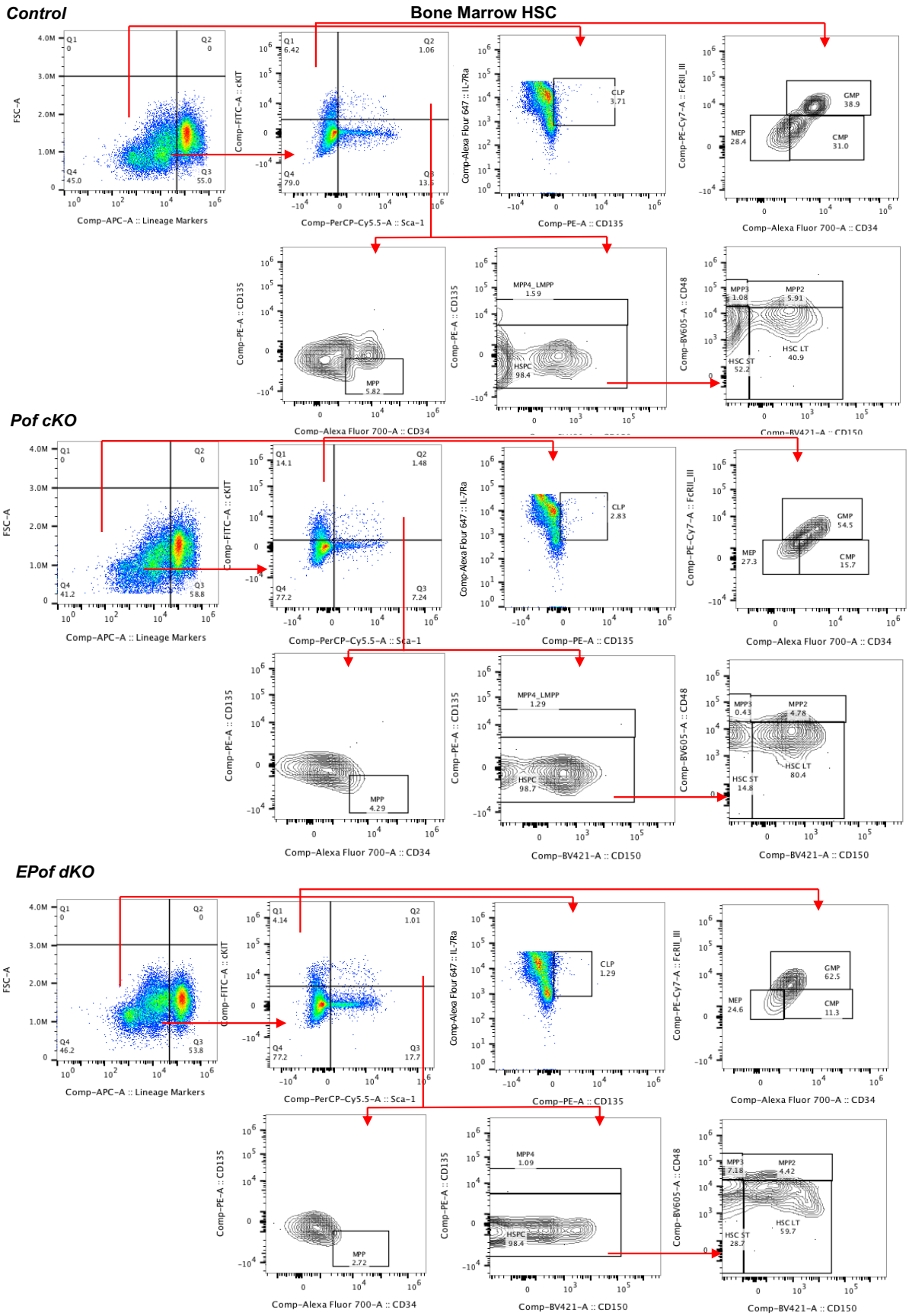
Control
Bone Marrow HSC
Q1 0
Q2 0
Q4 45.0
Q3 55.0
FSC-A
Comp-APC-A :: Lineage Markers
Q1 6.42
Q2 1.06
Q4 79.0
Q3 13.5
Comp-FITC-A :: cKIT
Comp-PerCP-Cy5.5-A :: Sca-1
CLP 3.71
Comp-Alexa Flour 647 :: IL-7Ra
Comp-PE-A :: CD135
GMP 38.9
MEP 28.4
CMP 31.0
Comp-PE-Cy7-A :: FcRII_III
Comp-Alexa Fluor 700-A :: CD34
MPP 5.82
MPP4_LMPP 1.59
HSPC 98.4
MPP3 1.08
MPP2 5.91
HSC LT 40.9
HSC ST 52.2
Comp-BV605-A :: CD48
Comp-BV421-A :: CD150
Pof cKO
Q1 0
Q2 0
Q4 41.2
Q3 58.8
Q1 14.1
Q2 1.48
Q4 77.2
Q3 7.24
CLP 2.83
GMP 54.5
MEP 27.3
CMP 15.7
MPP 4.29
MPP4_LMPP 1.29
HSPC 98.7
MPP3 0.43
MPP2 4.78
HSC LT 80.4
HSC ST 14.8
EPof dKO
Q1 0
Q2 0
Q4 46.2
Q3 53.8
Q1 4.14
Q2 1.01
Q4 77.2
Q3 17.7
CLP 1.29
GMP 62.5
MEP 24.6
CMP 11.3
MPP 2.72
MPP4 1.09
HSPC 98.4
MPP3 7.18
MPP2 4.42
HSC LT 59.7
HSC ST 28.7

Fig. S6 Gating strategy for BM hematopoietic cell subsets. (Related to Fig. 5)

Flow cytometric profiles of targeted cell populations were selected after gating on live cells using Zombie NIR dye using the Cytek™ Aurora flow cytometer from 7-8 weeks old, Control, Pof cKO and EPof dKO. HSPC populations were identified based on established gating strategies (*44, 45*):

LSK: Lin- cKit+ Sca1+,

Long-term hematopoietic stem cells (LT-HSC); Lin−Sca1+Kit+ CD150+CD135−,

Short-term hematopoietic stem cells (ST-HSC); Lin−Sca1+Kit+ CD150−CD135−,

Multipotent progenitors (MPP); Lin−Sca1+Kit+ CD150−CD135+,

Lymphoid primed multipotent progenitor cells (LMPP); Lin−Sca1+Kit+ CD135^{high},

Common lymphoid progenitors (CLP); Lin−KitintCD135+IL7Ra+,

Granulocyte/macrophage progenitors (GMP), Lin−Kit+Sca−FcRII/III+CD34+,

Megakaryocyte's erythrocytes progenitors' cells (MEP); Lin−IL-7R−c-kit+Sca-1−CD34−FcRII/III^{low}

Common myeloid progenitors (CMP); Lin−Kit+Sca−FcRII/III−CD34+,

Multipotent Progenitors cells 2 (MPP2); Lin−Kit+Sca+CD150+CD48+,

Multipotent Progenitors cells 3 (MPP3); Lin−Kit+Sca+CD150-CD48+

Multipotent Progenitors cells (MPP4); Lin−Kit+Sca+CD135+CD150-

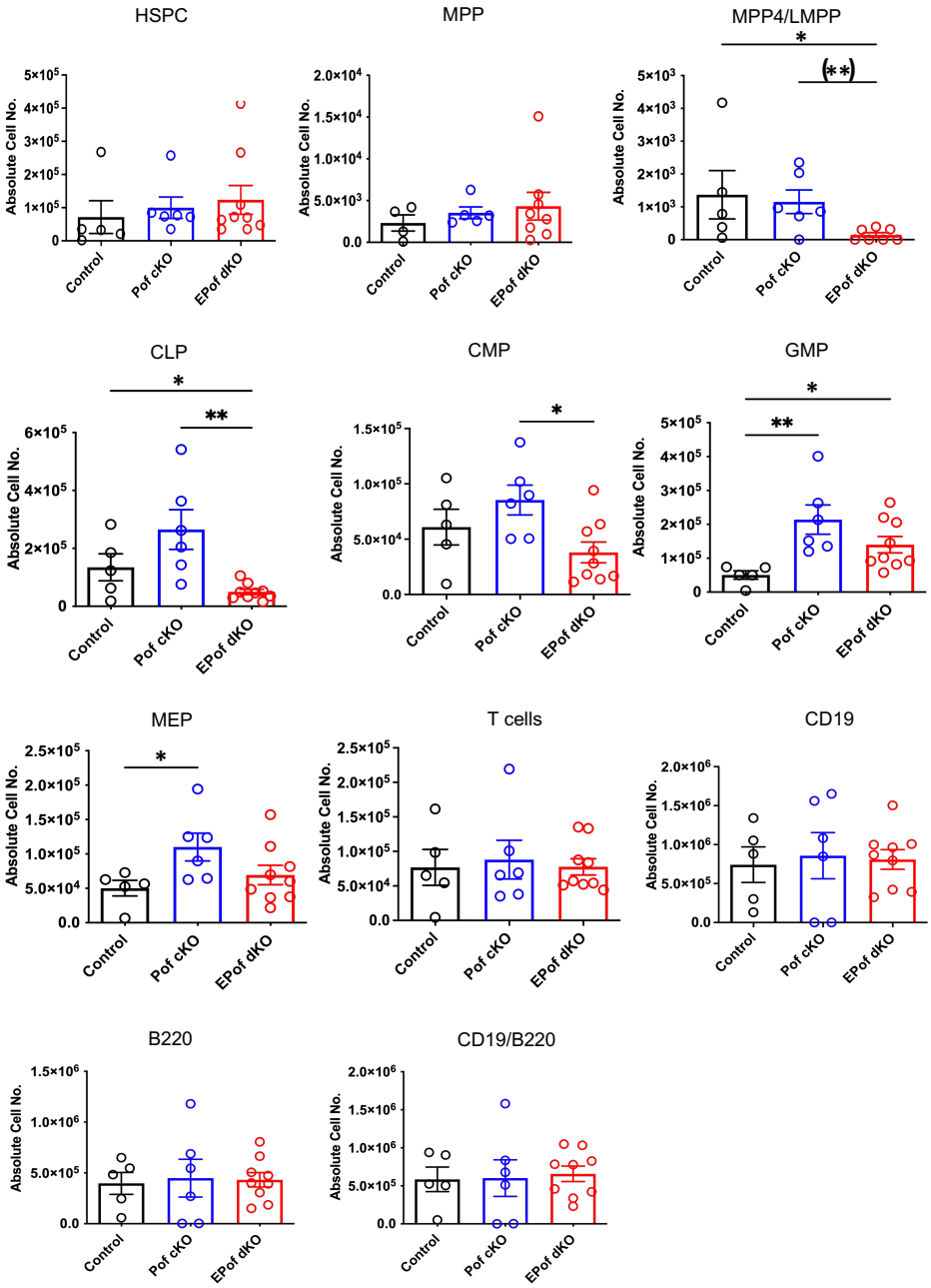

Fig. S7 Hematopoietic stem progenitors in Pof cKO and EPof dKO BM. (Related to Fig. 5)

Hematopoiesis, lymphoid and myeloid cell development were compared in Pof cKO versus EPof dKO versus Control mice with no *Vav1*-iCre. Each symbol represents a mouse of 7-8 weeks. Absolute cell numbers of different hematopoietic stem progenitor cells (HSPCs); multipotent progenitor (MPP) and multipotent progenitor-4 (MPP4)/LMPP cells, common lymphoid progenitor (CLP) common myeloid progenitor (CMP), granulocytes monocytes progenitor (GMP), megakaryocytes erythrocytes progenitors (MEP), T cells and B cells (B220/CD19) subsets.

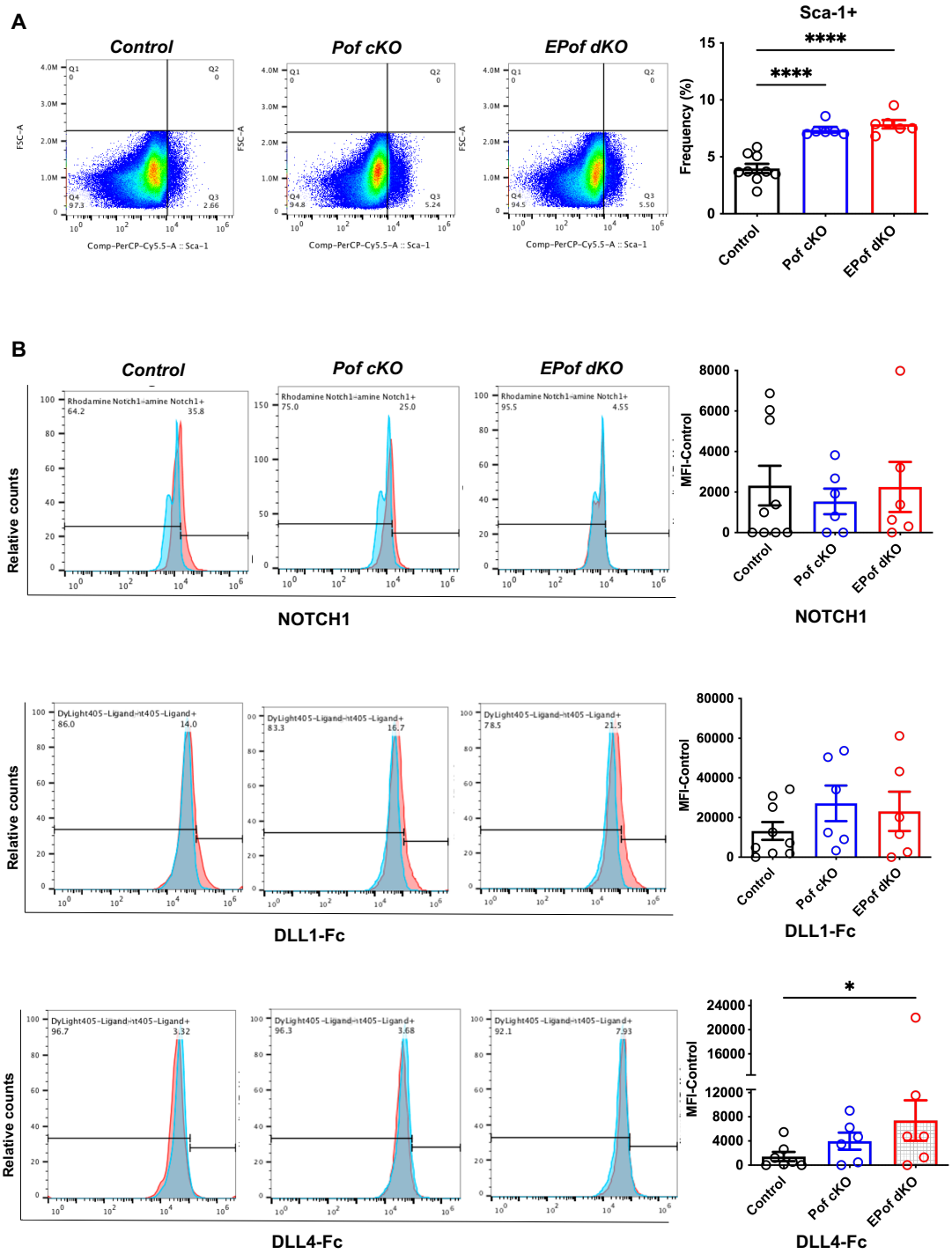

Fig. S8 Notch ligand binding to Lin-Sca1+ cells. (Related to Fig. 5)

Gating of Lin-Sca1+ cells and frequency (%) in triplicate samples from in BM from Control (n=3), Pof cKO (n=2) and EPof dKO (n=2) 6-7 weeks old mice. All replicates are shown. Flow cytometry profiles of NOTCH1 cell surface expression, and binding of DLL1-Fc or DLL4-Fc to Lin-Sca1+ cells from the same mice performed in triplicate.

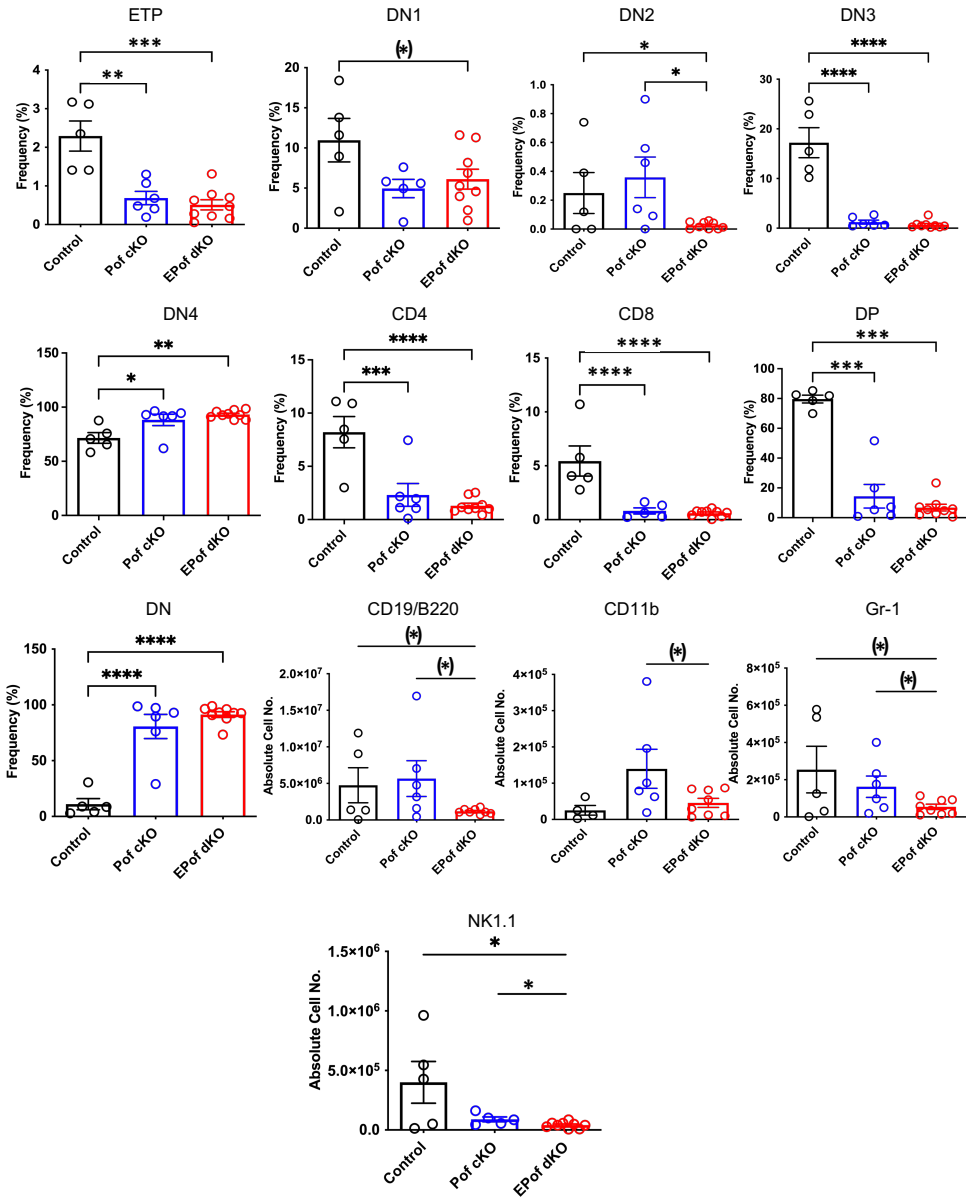

Fig. S9 Thymic immune cell subsets in Pof cKO and EPof dKO mice. (Related to Fig. 6)

Frequency(%) of different T-cell subsets; ETP(DN1 cells that were cKit/CD117+), and stages of different double negative (DN) T cells; CD44+CD25- (DN1), CD44+CD25+ (DN2), CD44-CD25+ (DN3), and CD44-CD25- (DN4) T cell progenitors, CD4, CD8, Double Positive (DP), Double negative (DN), and absolute numbers of B cells (B220/CD19), dendritic cells (CD11b/c), granulocytes (Gr-1) natural killer T-cells (NK1.1). Each symbol represents a mouse 7-8 weeks. Data are presented as mean SEM. *p <0.05, **p<0.01,***p<0.001, ,****p<0.0001 based on two-tailed Student t test and (*)p <0.05 based on one-tailed Student t test.

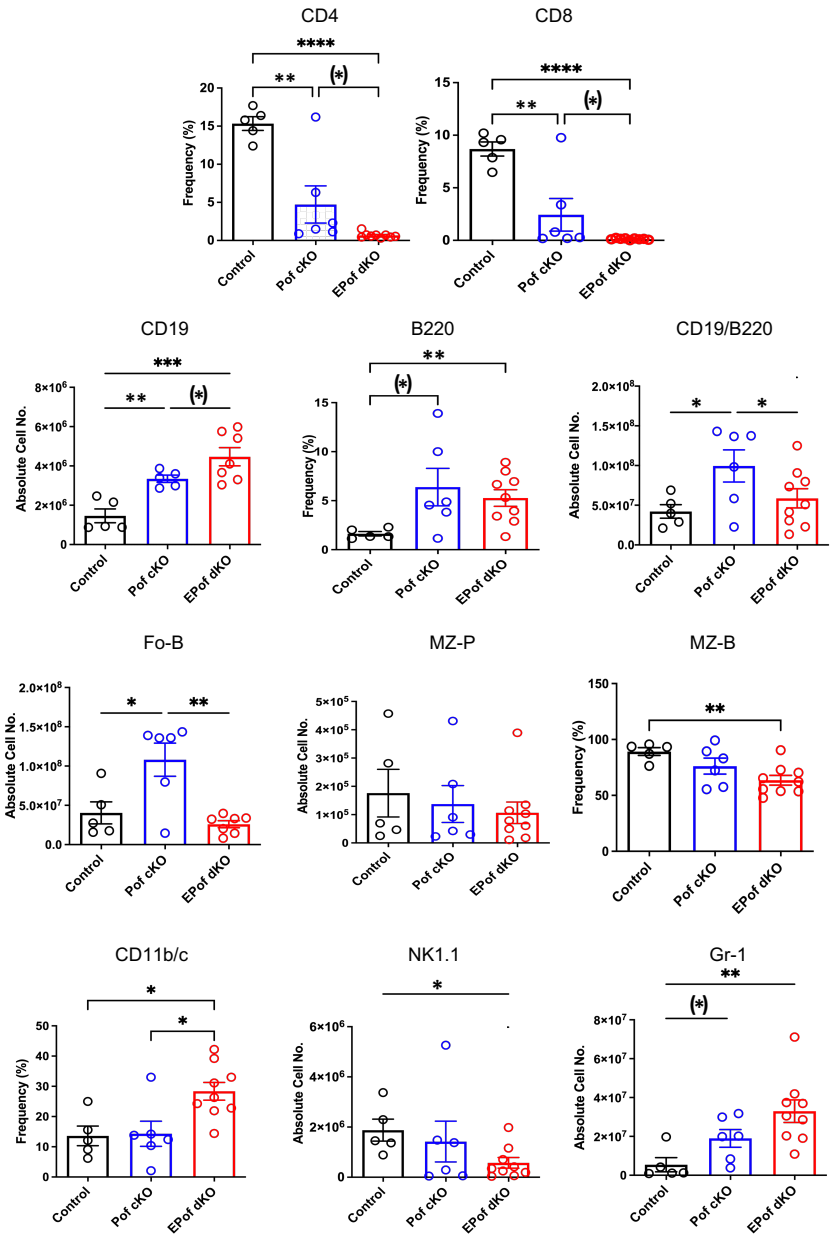

Fig. S10 Splenic immune cell subsets in Pof cKO and EPof dKO mice. (Related to Fig. 7)

Absolute cell numbers of CD19, B-cells (B220/CD19), follicular B cells (Fo-B), marginal zone precursors (MZ-P) cells, natural killer T cell (NK1.1) and granulocytes (Gr-1). Frequency (%) of splenic T-cell subsets; CD4, CD8 , B220, marginal zone-B (MZ-B), dendritic cells (CD11b/c). Each symbol represents a mouse 7-8 weeks. Data are presented as mean SEM. *p <0.05, **p<0.01,***p<0.001, ,****p<0.0001 based on two-tailed Student t test and (*)p <0.05 based on one-tailed Student t test.

Table S1 Primer sequences used in genotyping and qRT-PCR

Gene	Name	Sequence
Pofut1 F/del	PS644/Forward	*GGGTCACCTTCATGTACAAGTGAGTG*
	PS645/Reverse	*ACCCACAGGCTGTGCAGTCTTTG*
Pofut1 F/wt	FB21/Forward	*CCAGGCTGATCACTTCTTGG*
	FB22/Reverse	*CCCTGTCTCGAAAAAGCAAA*
Eogt	3rd loxF/Forward	*CCACCCGACCCCTGCCAGAACATAATGCTCTCTTGCATC*
	3rd loxR/Reverse	*GCTGTCGCCAGAGGAGAGAGTGGGTGCTTACTTAC*
	25307 Rv/Reverse	*CCAAGGCGGTCTTGGCCCAT*
Vav1-icre	FW internal/Forward	*CTAGGCCACAGAATTGAAAGATCT*
	RV Internal/Reverse	*GTAGGTGGAAATTCTAGCATCATCC*
	FW Transgene/Forward	*AGATGCCAGGACATCAGGAACCTG*
	RV Transgene/Reverse	*ATCAGCCACACCAGACACAGAGATC*
Hes1	Forward	*AAGGCAGACATTCTGGAAAT*
	Reverse	*GTCACCTCGTTCATGCACTC*
Hes5	Forward	*GGACCAGAGGATGAGCTCGTT*
	Reverse	*AGGAGGGAGCCTTCGGAAGA*
cMyc	Forward	*AGTGCTGCATGAGGAGACAC*
	Reverse	*GGTTTGCCTCTTCTCCACAG*
Deltex1	Forward	*CATCAGTTCCGGCAAGAC*
	Reverse	*ATGGTGATGCAGATGTCC*
CD25	Forward	*GGAATTGGTCTATATGCGTTGCTTA*
	Reverse	*CATGTCTGTTGTGGTTTGTTGCTCT*
Tcf7	Forward	*TCCGAGTACATGGAGAAGCC*
	Reverse	*GGGTAGGGCATGAGCAGATT*
Nrarp	Forward	*AGATACCGGATCCTCCGCTT*
	Reverse	*CCGGTAATGGTTGTTTGGCG*
Gapdh	Forward	*AAGGTCATCCCAGAGCTGAA*
	Reverse	*CTGCTTCACCACCTTCTTGA*
Hprt	Forward	*GGACCTCTCGAAGTGTTGGATAC*
	Reverse	*GCTCATCTTAGGCTTTGTATTTGGCT*

Table S2 Antibodies used in this work

Antibody	Fluorochrome	Isotype	Clone	Cat#	Company
CD4	PE	Rat IgG2a K	RM4.5	553048	BD Pharmingen
CD8a (ly2)	PE	Rat IgG2a K	53-6.7	553033	BD Pharmingen
CD45R/B220	PE-Cy7	Rat IgG2a, κ	RA3-6B2	103222	Biolegend
CD19	Alexa Flour 700	Rat IgG2a K	eBio1D3	56-0193-80	eBioscience
CD11b	FITC	Rat IgG2b K	M1/70	557396	BD Pharmingen
Ly6G/Ly6C	APC	Rat IgG2b K	RB6-8C5	108412	Biolegend
CD3	APC	Rat IgG2b K	145-2C11	553066	BD Pharmingen
CD11b	APC	Rat IgG2b K	M1/70	101212	Biolegend
Ter 119	APC	Rat IgG2b K	TER-119	116212	Biolegend
Gr-1	APC	Rat IgG2b K	RB6-8C5	108412	Biolegend
CD19	APC	Rat IgG2b K	MB19-1	17-0191-81	eBioscience
IL-7Ra/CD127	Alexa Flour 647	Rat IgG2b K	A7R34	135011	Biolegend
CD117/cKit	FITC	Rat IgG2b K	2B8	105805	Biolegend
CD135/flk2	PE	Rat IgG2b K	A2F10	135305	Biolegend
CD16/32 or FCRIII/II	PE-Cy7	Rat IgG2b K	93	101317	Biolegend
CD34	Alexa Fluor 700	Rat IgG2b K	RAM35	56-0341-82	Invitrogen
Sca-1	PerCp-Cy5.5	Rat IgG2b K	D7	108123	Biolegend
CD150	BV421	Rat IgG2b K	TC15-12F12.2	115925	Biolegend
CD48	BV605	Rat IgG2b K	HM48-1	103441	Biolegend
CD4	FITC	Rat IgG2b K	RM4.5	11-0042-85	eBioscience
CD44	PE-Cy7	Rat IgG2b K	IM7	25-0441-81	eBioscience
CD25	PerCPCy5.5	Rat IgG2b K	PC61	102029	eBioscience
CD117 (cKit)	APC	Rat IgG2b K	1B8	553356	BD Pharmingen
CD19	PE-Cy7	Rat IgG2b K	6D5	115520	Biolegend
NK1.1	PerCPCy5.5	Rat IgG2b K	PK136	61-5941-80	eBioscience
Ly6G/Ly6C	APC	Rat IgG2b K	RB6-8C5	108412	Biolegend
CD4	FITC	Rat IgG2b K	RM4.5	11-0042-85	eBioscience
NK1.1	PerCPCy5.5	Rat IgG2b K	PK136	61-5941-80	eBioscience
Ly6G/Ly6C	APC	Rat IgG2b K	RB6-8C5	108412	Biolegend
IgM	APC	Rat IgG2b K	II/4I	17579082	eBioscience

CD21/35	PerCPCy5.5	Rat IgG2b K	7E9	123415	Biolegend
CD23	Alexa Flour 700	Rat IgG2b K	B3B4	101631	Biolegend
CD45.2	PB	MOUSE SJL	104	109820	Biolegend
CD45.1	BV786	Mouse	A20	740889	BD Biosciences
AffiniPure F(ab9)2 Frag goat-anti-human IgG, Fcγ Frag Spec	APC	Goat-anti-human IgG		109-136-170	Jackson ImmunoResearch
AffiniPure F(ab9)2 Frag goat-anti-human IgG, Fcγ Frag Spec	DyLight 405	Goat-anti-human IgG		109-476-170	Jackson ImmunoResearch
Rhodamine Red-X-conjugated donkey anti-sheep IgG	Rhodamine Red-X	Donkey anti-sheep IgG		713-295-003	Jackson ImmunoResearch
CD16/ CD32 (mouse Fc block)		Rat anti-mouse	2.4G2	553142	BD Pharmingen
NOTCH1		Ag-purified polyclonal sheep	aa19-526		AF5267 (R&D Systems)